LUND UNIVERSITY

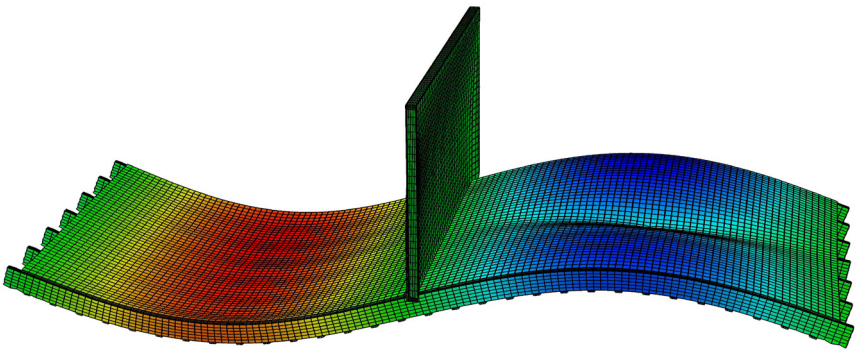

VIBRATION ANALYSES OF A WOODEN FLOOR-WALL STRUCTURE -Experimental and Finite Element Studies

JOEL EJENSTAM and OLA FLODÉN

Structural Mechanics

Master's Dissertation

Department of Construction Sciences
Structural Mechanics

ISRN LUTVDG/TVSM--11/5176--SE (1-62)
ISSN 0281-6679

VIBRATION ANALYSES OF A WOODEN FLOOR-WALL STRUCTURE - Experimental and Finite Element Studies

Master's Dissertation by

JOEL EJENSTAM and OLA FLODÉN

Supervisors

Kent Persson, PhD, and Anders Sjöström, MSc,
Div. of Structural Mechanics

Examiner:

Göran Sandberg, Professor,
Div. of Structural Mechanics

Printed by Wallin & Dalholm Digital AB, Lund, Sweden, May, 2011 *(Pl)*.

For information, address:
Division of Structural Mechanics, LTH, Lund University, Box 118, SE-221 00 Lund, Sweden.
Homepage: http://www.byggmek.lth.se

Preface

This Master's dissertation was carried out at the Division of Structural Mechanics at the Faculty of Engineering, Lund University. The work began in September 2010 and was finished in January 2011.

It would not have been possible to complete the dissertation without the help of our supervisors Ph.D. Kent Persson and M.Sc. Anders Sjöström at the Division of Structural Mechanics. We would like to thank Kent Persson for his advice and guidance during the construction and modeling phases of the project. We would also like to thank Anders Sjöström, who has been of great assistance with the experimental setup and the analysis of the results.

Finally, we would like to thank the staff at the Division of Structural Dynamics for welcoming us to the group and providing help when needed.

Lund, January 2011

Ola Flodén & Joel Ejenstam

Abstract

Changes in the Swedish construction code introduced in 1994 enabled the construction of wooden multistorey buildings. This resulted in an increased need for knowledge about wooden structures in the building industry. The main issue in wooden framed buildings is disturbing vibrations and noise which propagate throughout the construction.

It is valuable to be able to predict the behavior of future or existing structures. By creating and analysing calculation models, it is possible to obtain for example eigenfrequencies and the response of a specific load case of a structure. There is much experience in calculations for heavy constructions, but there is a lack of knowledge when it comes to establishing reliable calculation models of lightweight constructions.

This Master's dissertation contains experimental and finite element vibration analyses of a wooden full scale floor-wall structure. The floor structure was built in October 2010 at the Faculty of Engineering at Lund University, LTH. It was excited with harmonic loads from 15 to 400 Hz by a shaker and impulse loads made by hammer strokes, and the response was recorded with accelerometers. The experimental data was processed and evaluated with Matlab to obtain eigenfrequencies and mode shapes. Finite element modeling and analyses were performed with a software called Abaqus.

The objective of the project was to compile the eigenfrequencies and mode shapes of the floor structure from the retrieved experimental data and the finite element simulations. The aim was to establish a model that simulates the behavior of the real structure with good resemblance. The analyses were limited to eigenfrequencies below 100 Hz.

Measurements were carried out at different stages during the building phase, in order to see the effects on the eigenfrequencies when adding new parts to the structure. Being able to continuously compare the simulated and experimental results made the process of creating a well corresponding finite element model much easier. The final model shows a good resemblance to the real structure in terms of eigenfrequencies and mode shapes for the lower frequencies.

Contents

1. Introduction

1.1. Background

The use of wooden frameworks in buildings in Sweden was restricted to two-storey houses for almost the entire 20th century. The reason for this was a prohibition that followed a great fire in Sundsvall, 1888. The prohibition prevented the construction of wooden multistorey buildings, until it was revoked in 1994. The new Swedish construction code (BKR) introduced in 1994 were based on the functionality of the construction and enabled the building of multistorey wooden houses. Although a lot of knowledge and experience has been lost over the years, there are good role models both in Europe and North America to learn from. In the United States for example, 80-90 % of the multistorey buildings are made with wooden frames and there are over 70,000 wooden bridges.[6]

Wood is a sustainable and renewable construction material, and a resource that is plentiful in Sweden. There can be several advantages using wood as a building material. Research has shown that using wood instead of concrete in a building, will decrease the emissions of carbon dioxide significantly, because wood is a natural material and easily shaped and processed[7]. A building made out of wood will also have a lower demand for energy during its lifespan of service[8]. But there are naturally disadvantages as well. Due to the lightweight framework and construction, problems with sound transmission and vibrations will occur in the building if not treated properly. This is often accepted in a single family house, but in a block of apartments it can be an intolerable issue.[9]

In the process of planning a building, the dimensioning is usually performed accounting for static load cases whereas the influence of dynamic loads are neglected. Dynamic loads can be a hazard to the strength of the structure, but they can also create disturbing vibrations and noise in the building. The weight of the floor and wall structure of a building has a large impact to the acoustic insulation. A concrete frame building is much heavier and stiffer than a wooden frame building, which results in a good sound-proofing capacity. To achieve sufficient sound-proofing in a wooden building, special construction solutions have to be made.

The construction industry has a lot of experience and knowledge about the behavior of heavy concrete structures. Reliable simulation methods that are able to predict the behavior of a structure with high resemblance to reality have been developed.

It is important to gain this kind of knowledge about a construction already on the projecting state, to avoid structural errors that can be costly in the future. But the knowledge about lightweight structures is much more limited and the industry has a great need to increase this knowledge. One of the areas where there is a lot to be done is in the development of high resolution methods of prediction tools, for instance finite element models. If you can predict the vibrations and the acoustic behavior of a structure, the possibility to develop innovative solutions to such problems is increased. But there are difficulties when modeling lightweight structures, for instance due to the many joints and junctions and the orthotropic nature of wood. [9]

Disturbing noise levels from footfalls is the most common problem in wooden buildings. Another specific main problem is flanking transmissions, which means that vibrations propagate to load bearing walls and connecting rooms from the floor structure. The construction built in this project is intended to be used for studying these phenomena as well as airborne sound propagation through structures.

1.2. Objective and method

The objective of this project is to analyse the vibrations of a wooden floor structure that is subjected to harmonic and transient loads. The analyses will be performed both on an experimental structure and on a finite element model of the structure. The aim is to retrieve the eigenfrequencies and mode shapes from the experimental data and to create an FE-model that with satisfying resemblance simulates the behavior of the structure. The goal is to develop a model that is able to simulate eigenfrequencies and mode shapes up to approximately 100 Hz.

The vibrations of the floor structure are recorded using sensitive accelerometers and the obtained experimental data is processed and analysed with Matlab. The FE-model of the floor is created and post-processed in a software application for finite element analysis called Abaqus\CAE, whilst the actual calculations are carried out in Abaqus\Standard.

2. Theory of Structural Dynamics

2.1. Introduction

Vibrations appear in structures due to the presence of dynamic loads, i.e. loads that vary in time. These loads introduce new problems compared to the static case. When studying a structure that is subjected to a static load, a larger force will in general cause larger displacements and a more solid construction is therefore needed. The situation is not as trivial when dynamic loads are acting on the structure. In this case, the magnitude of the load might not be as important as the frequency it is varying with. For a load with an excitation frequency close to a so called natural frequency (or eigenfrequency) of the structure, the response can be significantly larger than for a load with the same magnitude but different frequency.

Vibrations can be described as the oscillations around the equilibrium of a structure, which is the position the structure returns to when no external loads are acting on it. The displacements around the equilibrium are measured in order to analyse the vibrations and can be viewed both as functions in the time domain and in the frequency domain. The last alternative can be useful when studying the dynamic behavior of a structure and is called the response spectrum. To convert a signal between the two domains a Fourier analysis algorithm such as FFT (Fast Fourier Transform) may be used. An example of a signal in the time domain and its response spectrum is shown in Figure 2.1.

When analysing a mechanical system there is always a question of how thorough you should be, how much can you idealize the system and still simulate its behavior? Except for all the assumptions about physical laws etc. you have to decide whether to view the system as continuous or discrete. It is practically impossible to analyze a complex structure as continuous and therefore it is discretized into a number of DOFs (Degrees Of Freedom). A degree of freedom describes either a displacement or a rotation and together they describe the behavior of the discretized system.

For references on this chapter and more information, see e.g. Chopra, Dynamics of Structures (1995).

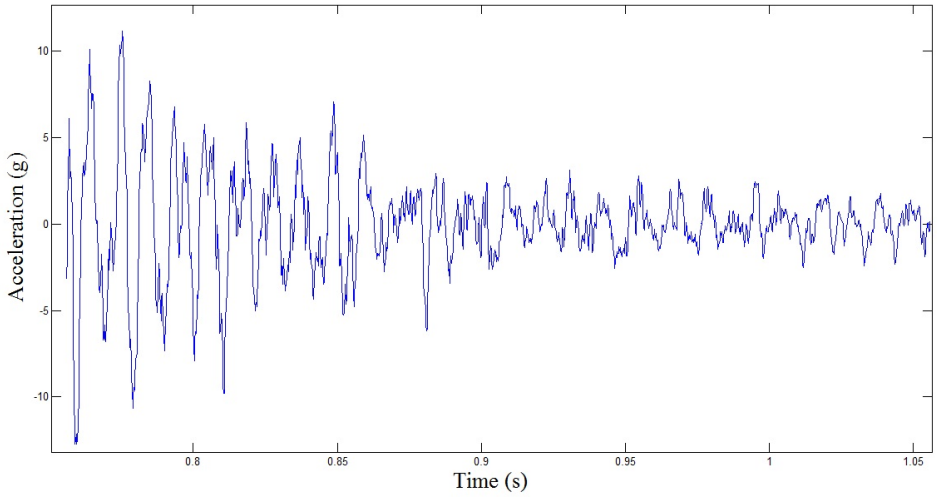

(a) Time domain.

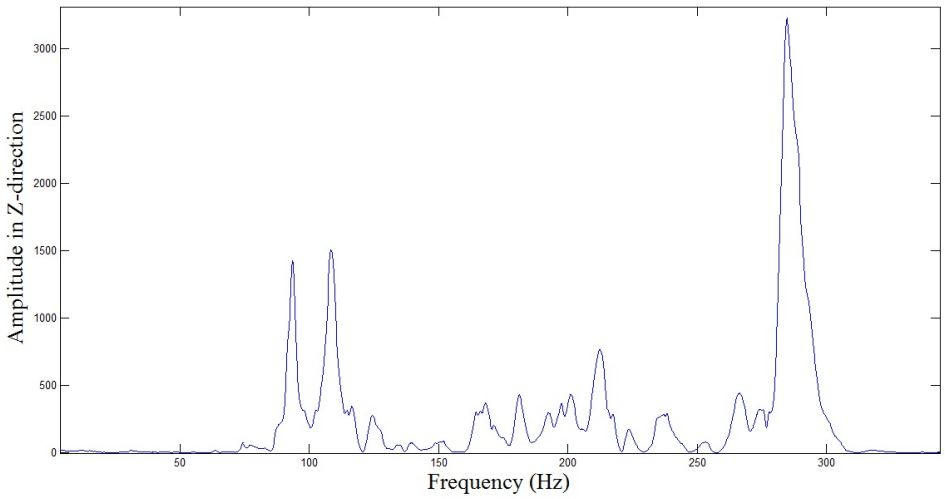

(b) Frequency domain.

Figure 2.1: A signal in time and frequency domain.

2.2. Equation of motion

The simplest way of modeling a dynamic system is to use a single-degree-of-freedom model (SDOF), which describes the system using only one degree of freedom. An example of such a system is illustrated in Figure 2.2. It consists of a mass m connected to the wall with a spring and a damper (both massless). The mass moves frictionless in the horizontal direction and the degree of freedom is in this case the displacement u from the equilibrium. A time-dependent load $p(t)$ excites the mass.

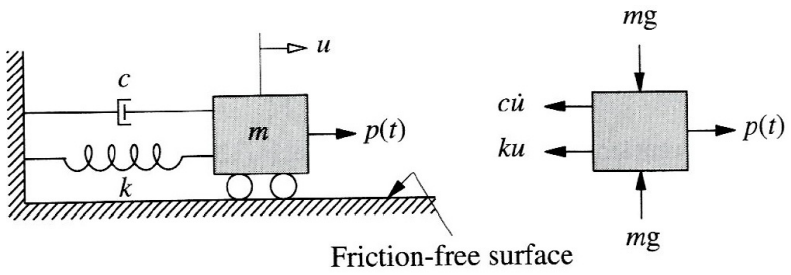

Figure 2.2: A SDOF system.[1]

Studying the free body diagram in figure 2.2 and using Newton's second law of motion leads to Eq. 2.1.

$$p(t) - c\dot{u} - ku = m\ddot{u} \tag{2.1}$$

Rearranging the terms in Eq. 2.1 results in the equation of motion for a SDOF model:

$$m\ddot{u} + c\dot{u} + ku = p(t) \tag{2.2}$$

The displacement $u(t)$ is given by solving the equation of motion.

In case of a more complex structure it is necessary to include more degrees of freedom to describe the dynamic behavior. This results in a multi-degree-of-freedom model (MDOF). For a system subjected to small displacements (neglecting any non-linear behaviour), the equation of motion for a SDOF system can be extended to the multi-dimensional case, see Eq. 2.3.

$$\mathbf{M\ddot{u}} + \mathbf{C\dot{u}} + \mathbf{Ku} = \mathbf{P}(t) \tag{2.3}$$

$\mathbf{M}$ is the mass matrix, $\mathbf{C}$ the damping matrix and $\mathbf{K}$ the stiffness matrix. $\mathbf{u}$ is the displacement vector and $\mathbf{P}$ the load vector. If there are n degrees of freedom in the model, the matrices will be of size n×n and the vectors n×1.

2.3. Modal analysis

A structure has an infinite number of eigenfrequencies. These are the frequencies the structure will oscillate at when it is allowed to vibrate without the influence of any external loads. Each eigenfrequency has a corresponding mode shape. If the structure is curved into a mode shape and released from rest, it will oscillate at the

corresponding frequency.

Studying a structure in free vibration (no external loads) and assuming that no damping is present, the equation of motion is reduced to:

$$\mathbf{M\ddot{u}} + \mathbf{Ku} = 0 \tag{2.4}$$

To solve Eq. 2.4, a harmonic solution is assumed:

$$\mathbf{u}(t) = Acos(\omega t)\Phi + Bsin(\omega t)\Phi \tag{2.5}$$

Differentiation of $u(t)$ and insertion into Eq. 2.4 gives the eigenvalue problem in Eq. 2.6.

$$(\mathbf{K} - \omega^2\mathbf{M})\Phi = 0 \tag{2.6}$$

$$\Rightarrow \ det(\mathbf{K} - \omega^2\mathbf{M}) = 0 \ \Rightarrow \omega_1, ..., \omega_n$$

When a structure is discretized into n degrees of freedom, there are n eigenvalues. Each eigenvalue ω_i has a corresponding eigenvector Φ_i. These are the angular eigenfrequencies and mode shapes of the structure. Together, an eigenvalue and eigenvector pair form a solution $\mathbf{u}(t) = A \cdot cos(\omega_i t)\Phi_i + B \cdot sin(\omega_i t)\Phi_i$ that satisfies the differential equation. A and B are given by the initial conditions $\mathbf{u}(0) = \mathbf{u}_0$ and $\dot{\mathbf{u}}(0) = \dot{\mathbf{u}}_0$. The mode vectors form an orthogonal basis and the solution can be expressed as a sum using all eigenvalues and eigenvectors:

$$\mathbf{u}(t) = \sum_{1}^{n} q_i(t)\Phi_i \tag{2.7}$$

$$q_i(t) = A_i cos(\omega_i t) + B_i sin(\omega_i t)$$

2.4. Steady-state vibrations

When a structure is excited with a harmonic load, it will after a starting transient phase oscillate with the frequency of the load. This is called a steady-state response.

Applying a harmonic load to the undamped system gives the following equation of motion:

$$\mathbf{M\ddot{u}} + \mathbf{Ku} = \mathbf{P}(t) \tag{2.8}$$

$$\mathbf{P}(t) = \mathbf{P}_0 sin(\omega t)$$

By using modal coordinates, $\mathbf{u}(t) = \sum_1^n q_i(t)\Phi_i$, and multiplying with Φ_r^T from the left, Eq. 2.9 is obtained.

$$\sum_1^n \Phi_r^T \mathbf{M}\Phi_i \ddot{q}_i(t) + \sum_1^n \Phi_r^T \mathbf{K}\Phi_i q_i(t) = \Phi_r^T \mathbf{P}(t) \tag{2.9}$$

The eigenvectors are orthogonal in the scalar products $\Phi_r^T\mathbf{M}\Phi_i$ and $\Phi_r^T\mathbf{K}\Phi_i$, hence only terms with $i = r$ are non-zero. This results in n uncoupled equations of the form:

$$M_i\ddot{q}_i(t) + K_i q_i = P_i(t) \tag{2.10}$$

$$M_i = \Phi_i^T\mathbf{M}\Phi_i,\ K_i = \Phi_i^T\mathbf{K}\Phi_i,\ P_i = \Phi_i^T\mathbf{P}(t) = P_{0i}sin(\omega t)$$

Insertion of a harmonic trial solution $q_i(t) = q_{0i}sin(\omega t)$ gives the following result:

$$q_{0i} = \frac{P_{0i}}{M_i}\frac{1}{\omega_i^2 - \omega^2} \tag{2.11}$$

$$\omega_i = \tfrac{K_i}{M_i}$$

The result shows that an excitation frequency ω equal to an eigenfrequency will give an infinite amplitude. This is of course not the case in reality, any kind of damping in the structure will prevent such a phenomenon. But if the level of damping is not very high, there will still be a peak in the displacement amplitude spectrum at the eigenfrequencies.

2.5. Damping

Damping is included in models to represent the energy dissipation in structural dynamics and is always present in some kind. It can for example be friction in joints or internal properties of materials.

If $p(t) = 0$ in Eq. 2.2, the equation of motion can be rewritten as:

$$\ddot{u} + 2\zeta\omega_n\dot{u} + \omega_n^2 u = 0 \tag{2.12}$$

$$\omega_n = \sqrt{\tfrac{k}{m}},\ \zeta = \tfrac{c}{2m\omega_n}$$

ζ is the so called damping ratio and ω_n the eigenfrequency for the undamped case. Solving the equation gives the response for a damped free vibrating structure:

$$u(t) = e^{-\zeta\omega_n t}[u(0)cos(\omega_D t) + \frac{\ddot{u}(0) + \zeta\omega_n u(0)}{\omega_D} sin(\omega_D t)] \tag{2.13}$$

$$\omega_D = \omega_n\sqrt{1-\zeta^2}$$

ω_D is the eigenfrequency for damped vibrations and is related to ω_n by a factor $\sqrt{1-\zeta^2}$. For relatively small damping ratios ($\zeta < 0.2$), $\omega_D \approx \omega_n$. An example of a damped free vibration is plotted in Figure 2.3.

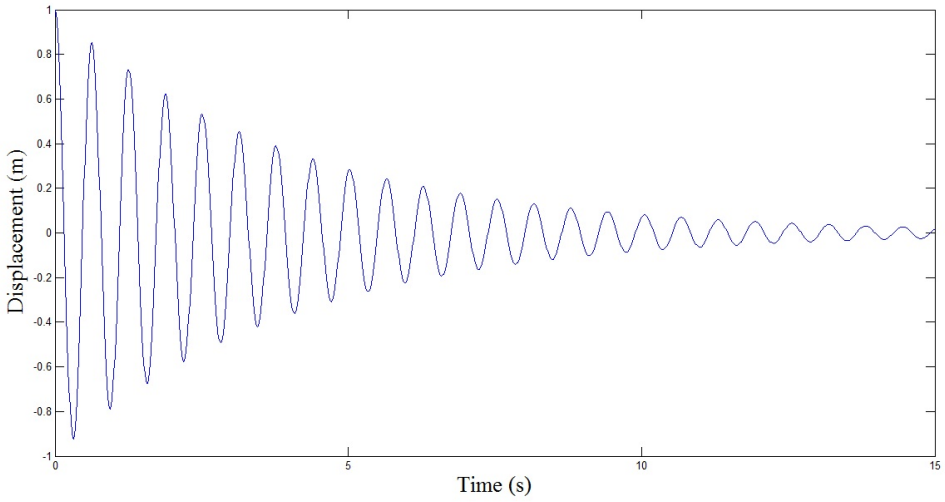

Figure 2.3: A damped free vibration.

As mentioned in the steady-state vibrations section, the response amplitude of a harmonic load will not go to infinity if there is damping in the structure. The amplitude of the peak in the frequency response spectrum will depend on the damping ratio. Figure 2.4 shows the deformation response factor for frequencies around an eigenfrequency. The deformation response factor is a quota between the amplitude of the dynamic response for a harmonic load and the amplitude of the static response for a static load of the same magnitude.

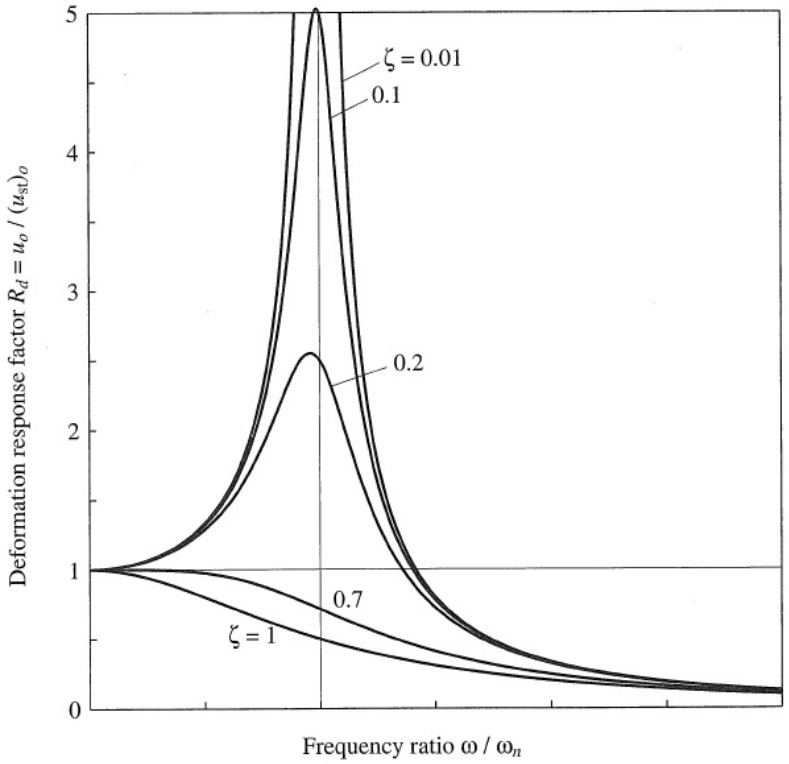

Figure 2.4: The deformation response factor for different damping ratios.[1]

For a MDOF model, a damping matrix needs to be constructed. It is not as simple as constructing the stiffness matrix, which is built by considering the stiffness properties of individual elements. For example, the damping properties of materials are not as well established and also the energy dissipation in connections needs to be taken into account. Instead, the damping matrix may be constructed from the modal damping ratios of the structure. There are two types of damping matrices, classical and non-classical. The difference is that classical damping matrices are diagonal and non-classical damping matrices are not. A diagonal matrix makes it possible to separate the equation system into n uncoupled equations, like in the undamped case, and it is therefore possible to perform classical modal analysis of the structure.

The method of constructing the damping matrix used in this project is Rayleigh damping, which gives a classical damping matrix. The Rayleigh damping matrix is a linear combination of the mass matrix and the stiffness matrix, as shown in Eq. 2.14.

$$\mathbf{C} = a_0\mathbf{M} + a_1\mathbf{K} \tag{2.14}$$

Using the formula for the damping ratio stated in Eq. 2.12, it can be shown that the damping ratio of the nth mode is given by:

$$\zeta_n = \frac{a_0}{2\omega_n} + \frac{a_1\omega_n}{2} \tag{2.15}$$

a_0 an a_1 can be obtained from two known damping ratios ζ_i and ζ_j. If ζ is assumed to be constant in modes i and j, a_0 and a_1 is given by Eq. 2.16 and 2.17.

$$a_0 = \zeta\frac{2\omega_i\omega_j}{\omega_i + \omega_j} \tag{2.16}$$

$$a_1 = \zeta\frac{2}{\omega_i + \omega_j} \tag{2.17}$$

The damping as a function of frequency in the case of constant damping ratios in modes i and j is shown in Figure 2.5. The mass matrix damps the lower frequencies and the stiffness matrix damps the higher frequencies.

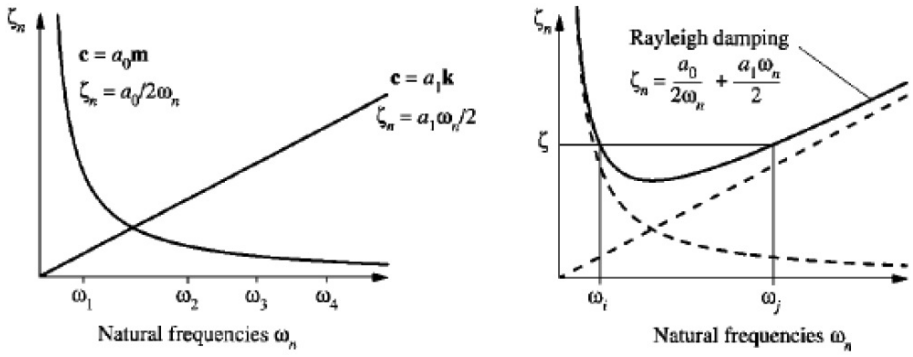

Figure 2.5: Damping ratio vs frequency for Rayleigh damping.[1]

2.6. RMS-value

The RMS-value (Root Mean Square value), defined in Eq. 2.18, is used to create an average magnitude of a signal over time. Since the sign of the displacements varies in time for vibrations, it is suitable to use the RMS-value instead of the mean value.

$$u_{RMS} = \sqrt{\frac{1}{\Delta t}\int_{t_0}^{t_0+\Delta t} u^2(t)\,dt} \tag{2.18}$$

3. Design and Construction

3.1. The building site

The wooden floor-wall structure was built in a transmission laboratory in the basement of the V-building at Lund University. The laboratory consists of two rooms separated by a 1.2 m thick concrete wall. The wall has an opening 0.5 m above the floor with a size of 4×2.5 m^2. The rooms have an equal size of 6.5×5.6×3.4 m^3 and the floor, walls and ceilings are made of concrete. The laboratory is sketched in Figure 3.1.

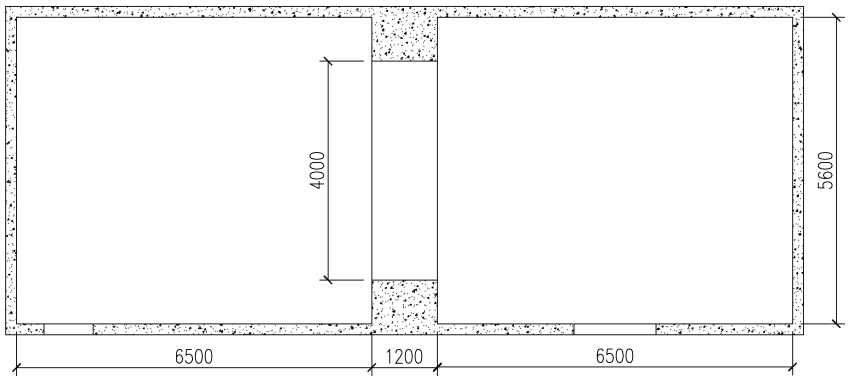

(a) Overview sketch of the two rooms.

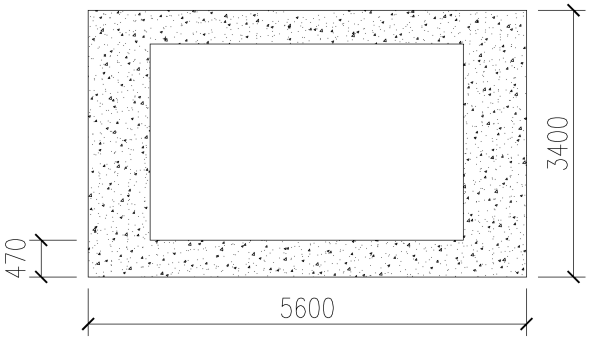

(b) Section sketch of the wall and cavity connecting the rooms.

Figure 3.1: Sketches of the transmission laboratory.

3.2. Design

The design of the floor-wall structure was made with the intention to resemble a section of a wooden building as they are built in reality. The dimensions of the structure was built as big as allowed by the size of the laboratory. The floor structure was built using wooden beams as the load-bearing components, particle boards as the floor surface and with secondary spaced boarding attached to the underside of the beams. The floor is simply supported at both ends and at the midspan. The midspan support is placed in the wall opening and the floor extends equally into both rooms. The total length is 9.3 m and the span between the outer supports is 9.0 m. The width of the floor is 3.6 m. A wooden frame wall is placed over the midspan support with dimensions suited to cover the opening in the concrete wall. The outer frame of the wall is fixed to the surrounding concrete wall and the underlying wooden floor. The wall is filled with insulation between the wooden beams and covered with plaster boards. The cavity under the floor at the midspan support is also filled with insulation.

3.3. Materials

Data for all structural parts and materials are shown in table 3.1. The load bearing wooden beams are quality classed with the Swedish standard K24. The midspan support consists of a steel T-beam lying upside down directly on the concrete in the gap between the rooms. On the end supports the beams are resting on short steel L-beams that are placed on concrete pillars.

Part	**Material**	**Dimensions (mm)**	**Quantity**
Supporting beam	Wood (K24)	45×220×6200	11
Joist/Top plate	Wood	45×90×4000	2
Wall beam	Wood	45×90×2100	9
Spaced boarding	Wood	28×70×3600	30
Floor board	Particle board	22×600×2400	23
Wall board	Plaster board	13×1200×2400	6
Insulation	Glass wool	95×565×1170	12
End support pillar	Concrete	h=500	14
End support L-beam	Steel	h=30, t=3, l=50	14
Mid. Support T-beam	Steel	h=50, w=100, t=5, l=3800	1
Tie plate	Steel	2×120×300	14
Bracket (tie angle)	Steel	3×70×(90+90)	24

Table 3.1: Building parts and materials used in the construction.

3.4. Construction

The longest beams available in stores are 6.2 m long and to create a 9.3 m floor two beams had to be joined. One and a half 6.2 m beams were joined using a tie plate at both sides of the beams. This resulted in 9.3 m long beams. The joint is shown in figure 3.2.

The spacing between the beams in both floor and wall is according to the cc 600 standard, which means that the beams were placed with a distance of 600 mm from center to center. The outer supports were placed in two parallel lines 9.0 m apart, to support both ends of the beams. The distance between the concrete pillars on each line is the same as the distance between the beams, 600 mm. To stabilize the supports, which have rough and uneven base surfaces, they were fixed to the concrete floor using grout, see Figure 3.3.

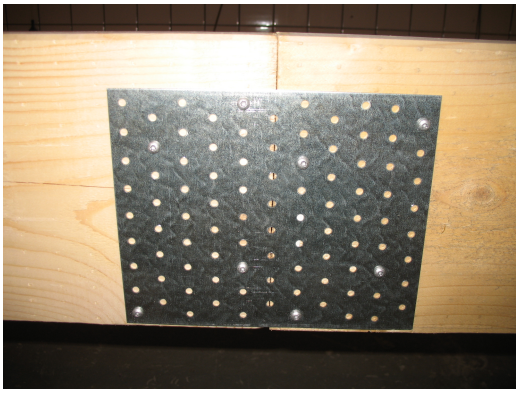

Figure 3.2: Beam joined with a tie plate.

Figure 3.3: A support fixed to the floor.

First the beams were placed on the supporting pillars, then the secondary spaced boarding was screwed to the bottom of the beams. They were placed perpendicular to the beams with a center distance of 300 mm. The floor structure with supporting beams and secondary spaced boarding is shown in figure 3.4.

The particle boards were also placed perpendicular to the supporting beams. To cover the beam structure, 15 lines of boards were required with one and a half board in each line. This gave a 9.0 m long and 3.6 m wide floor. The sides of the particle boards are flanged to create a better connection. All connections in between boards and to the beams were glued together with wood glue. The outer sides of the boards were screwed to the beams with five screws per side and the middle of the boards were screwed to the underlying beams with three screws. The complete floor is shown in figure 3.5.

Figure 3.4: The beams with secondary spaced boarding.

Figure 3.5: The complete floor.

The wall separating the two rooms was built on top of the floor. The top plate and the side beams of the wall were glued and firmly screwed to the surrounding concrete wall and the sill was attached to the floor structure below with two screws per support beam. Vertical beams were fixed to the inside of the frame using a bracket in each corner. The vertical beams were placed above each of the supporting beams. The framework is shown in figure 3.6.

Figure 3.6: The framework of the wall.

Plaster boards were attached to one side of the frame with 200 mm between the screws along the edges of the boards and 300 mm along the center line of the board. Insulation was placed to fill the holes between the beams and finally plaster boards were also attached to the other side of the framework. The plaster boards and insulation are shown in figure 3.7 and the complete structure in figure 3.8.

Figure 3.7: Insulation and plaster boards.

Figure 3.8: The complete structure.

4. Measurements

4.1. Introduction

Measurements were carried out at different stages throughout the construction phase to make it possible to compare measurements of parts of the structure with analysis results. Modeling of a complex structure such as the floor-wall structure studied in this project is very difficult. If the results obtained from simulations does not resemble the experimental values, it can be hard to analyse what causes the errors since there are many possible sources of error. Measurements were performed in four phases of the building process; a floor beam, the floor structure with and without particle boards and the complete floor-wall structure. The motion of the structure was measured in the vertical direction since those displacements were assumed to be the largest since the loads were applied vertically. Accelerometers were used to measure the acceleration.

The objective of the measurements is to obtain information about eigenfrequencies, mode shapes and damping of the structure. Processing and analyzing measurement data is time-consuming though, and therefore only the most important data processing were made. Eigenfrequencies were evaluated for all structures, but not for all measurements and accelerometers. Mode shapes were only evaluated for the complete floor-wall structure and damping was only evaluated for the floor structure without particle boards. The analyses were limited to frequencies below 100 Hz.

All coordinates for accelerometer and excitation positions on the assembled structures are given in Appendix A. The origin is defined in the figures under the experimental setup sections in this chapter. The y-axis is chosen to be aligned with the longitudinal direction of the floor beams and the x-axis perpendicular to the y-axis.

4.2. Equipment

For the measurements on a single beam, a measurement system with four channels was used. This system is unable to read data simultaneously on all four channels, and it is therefore impossible to determine mode shapes of the structure. During the experiments the software was malfunctioning. Although some data was unusable, the saved data was sufficient to determine the eigenfrequency.

All measurements on the assembled structures were done by a larger measurement

system with 32 channels. This system is able to read data simultaneously on all channels and the data from those measurements can consequently be used to analyse the mode shapes of the structure. The system consists of:

- 26 accelerometers of type *Analog Devices ADXL202E* which measures accelerations in two axes in the interval ±2 g with a resolution of 315 mV/g.
- 8 accelerometers of type *Analog Devices ADXL203* which measures accelerations in two axes in the interval ±1.7 g with a resolution of 1000 mV/g.
- Two coupling boxes with 16 input channels and 32 output channels to divide signals into x- and y-axis signals. They also act as power supply for the accelerometers.
- Two 16 bit A/D converter boards of type *Spectrum M2i.4711* with 16 synchronous channels and a maximum sampling rate of 100 kS/s.
- *Spectrum SBench 6* measurement software with ability to for example display, analyze and export data.

To excite the structures, both transient and harmonic loads were applied (harmonic loads were only applied to the floor structure with particle boards and the complete floor-wall structure). Transient loads were applied by simply striking the structure with a rubber mallet and harmonic loads were applied with a shaker system consisting of the parts listed below.

- Shaker, Goodman's Vibrators Ltd V50.
- PC to generate sinus waves used as input signal.
- Amplifier, Sentec ACM1, used to amplify input signal.
- Force sensor, Brüel & Kjær 8200.
- Power supply to force sensor, Brüel & Kjær 2805.
- Oscilloscope and voltmeter to observe output from the force sensor and input voltage to the shaker.

The shaker is similar to a loudspeaker with a rod attached to the membrane. The other end of the rod was attached to the structure with the force sensor in between. The input signal to the shaker was a five minute long sound file consisting of a sine wave which starts at a frequency of 15 Hz and then increases linearly in time up to 400 Hz at the end of the file.

The computers with some of the instruments is shown in Figure 4.1 and the shaker attached to the floor in Figure 4.2.

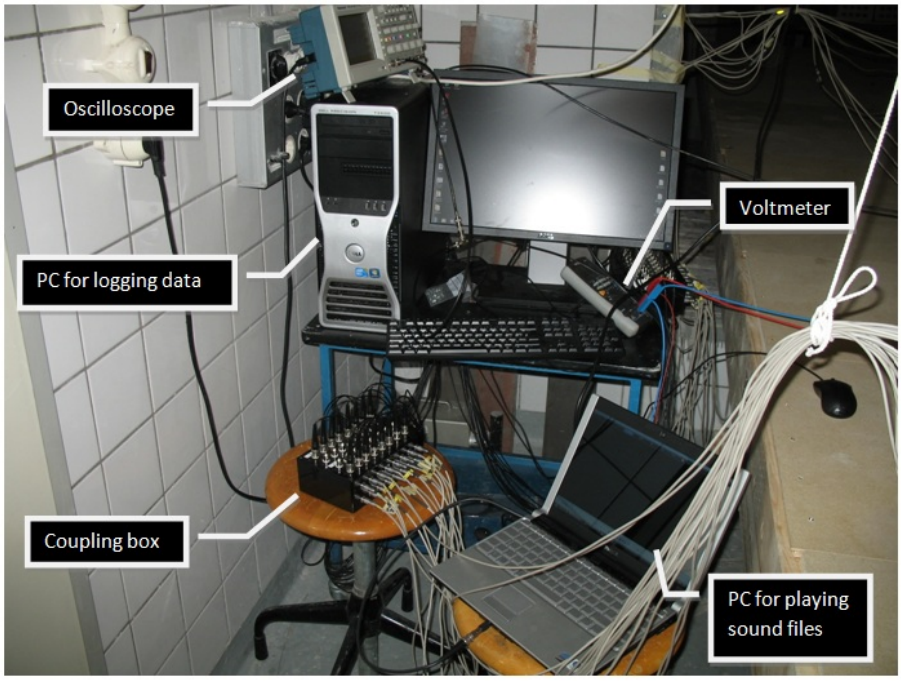

Figure 4.1: Experimental setup for the measurement system with 32 channels and the shaker system.

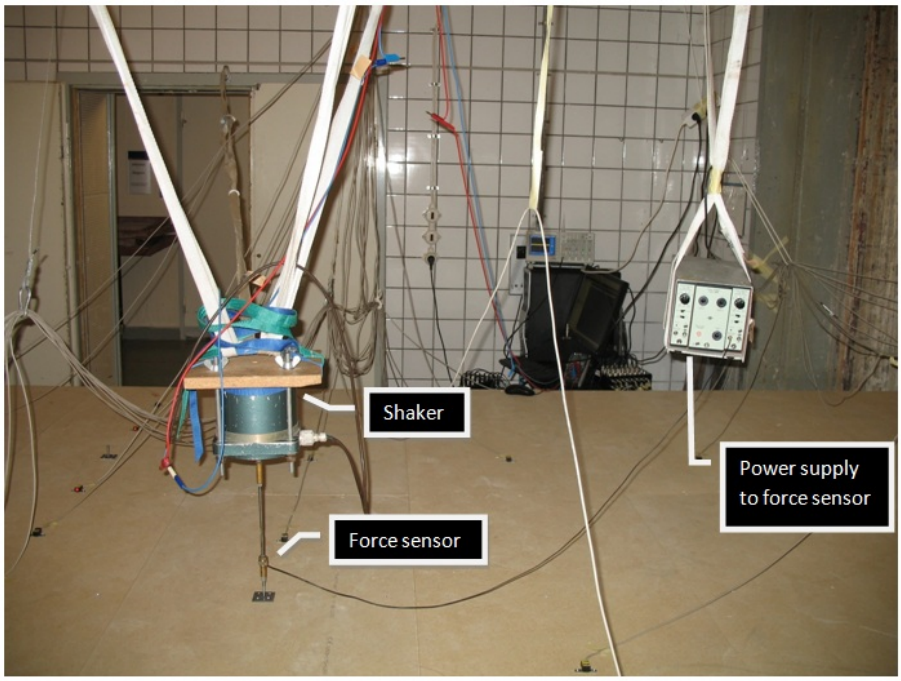

Figure 4.2: The shaker system attached to the floor.

4.3. Analysis methods

The Matlab code for processing the raw data and analysing the frequency sweep signals was provided by Anders Sjöström at the Division of Structural Mechanics. The remaining code was written by the authors.

4.3.1. Eigenfrequencies

The eigenfrequencies were obtained from the measurements of both harmonic and transient excitations. For the transient measurements, the eigenfrequencies were obtained by performing an FFT-analysis of the data and studying the frequency spectrum.

The harmonic frequency sweep measurements were transformed into frequency spectrums of the acceleration amplitude. The signal was divided into intervals containing a certain number of oscillation periods. The frequency and RMS-value of the acceleration were determined for each interval. The RMS-value was scaled with the signal from the force sensor and plotted versus frequency in order to determine the eigenfrequecies of the structure. An example can be seen in Figure 4.3. By using a fixed number of periods in each interval, the length of time of the intervals is reduced as the frequency increases. This makes the resolution better for higher frequencies.

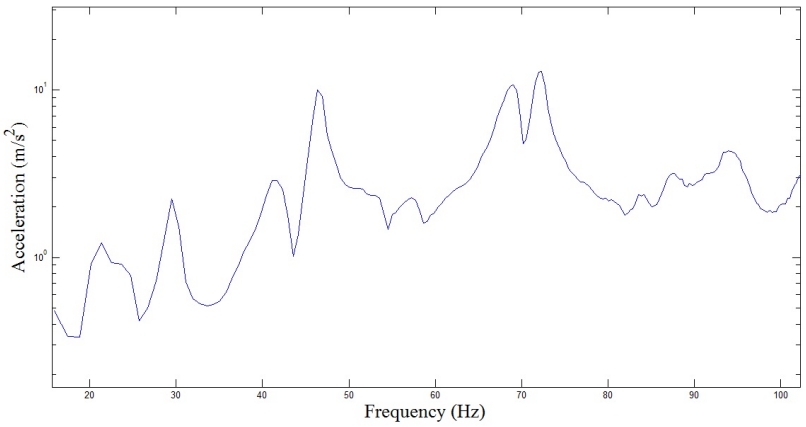

Figure 4.3: Example of an amplitude spectrum from a frequency sweep.

4.3.2. Mode shapes

The displacement of the structure was analysed for the frequencies with the largest peaks in the frequency spectrum. The frequency sweep signals were filtered just to contain frequencies of narrow intervals around the eigenfrequencies. By extracting the accelerations from all accelerometers at a certain sample when the structure is

oscillating with an eigenfrequency, the mode shapes were obtained.

The mode shapes were plotted by using the extracted vectors of accelerations and assuming the accelerations to be zero over the midspan support and at the four corners of the floor. The accelerations for the rest of the structure were obtained by linear interpolation.

4.3.3. Damping

In Eq. 2.14 it can be seen how the amplitude of an oscillation decays as a function of the damping ratio, ζ. By fitting functions of the form $y = Ae^{-\zeta t}$ to the amplitude of the transient measurements, estimations of the damping ratio are obtained. An example of such a function adapted to measurement data is shown in Figure 4.4. The fitting is performed with the least square value of the errors as minimization objective function. The amplitude values which the function is fitted to are picked by hand. to represent the amplitude of the signal with regular time intervals between the points. Eq. 2.14 only states the solution for a specific mode and in this case there are many active modes in the oscillations. Since only frequencies below 100 Hz were examined in this project, the transient time signals were filtered through a low pass filter with a cut off frequency of 100 Hz before the fitting was done. This gives a damping ratio that is in some sense an average for all modes below 100 Hz. It could have been done with better precision by filtering through the frequencies around one mode at a time, but since the objective was to find a damping ratio with an accurate order of magnitude to be used in the finite element modeling, it was unnecessary to perform any more advanced analyses.

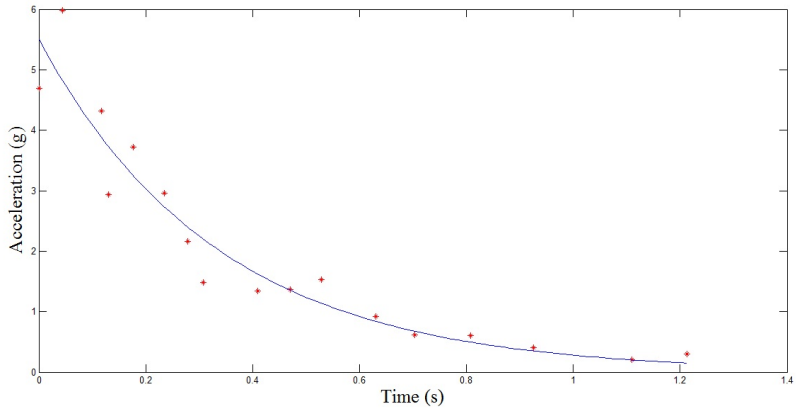

Figure 4.4: An exponential function (blue line) fitted to measured acceleration amplitudes (red points).

4.4. A single beam

Measurements on a single beam were carried out with the objective to establish two important material properties of the construction wood, the Young's modulus E and the density ρ. Wood is an anisotropic material with different elastic properties in the fiber direction than perpendicular to the fibers. The fibers are almost aligned with the longitudinal direction of a beam and stresses and strains mainly develop in that direction when a simply supported beam is oscillating. Consequently, it is more important to have an accurate value of the Young's modulus in the fiber direction and the measurements were therefore focused on determine that parameter. The Young's modulus in the other directions, the shear parameters and the Poisson's ratios are obtained from literature.

The construction wood was delivered dry and stored indoors before being used. The measurements were carried out in an indoor climate during the autumn and therefore the moisture content was assumed to be at most 12 %. However, no measurements were done to determine the actual moisture content.

The density was established by simply weighing the beams and dividing by the volume. Four different (unjointed) beams were weighed, resulting in an average value of the mass, $m = 26.53$ kg. The volume of a beam is $V = 6.2 \times 0.22 \times 0.045 = 0.0614$ m^3. Hence, the density is $\rho = 26.53/0.0614 \approx 432$ $\mathrm{kg/m}^3$.

The Young's modulus was determined by measuring the eigenfrequency of an oscillating simply supported beam. The lowest eigenfrequency of a simply supported beam is given by Eq. 4.1. When the eigenfrequency is known, the Young's modulus can be derived by

$$f_0 = \frac{\pi}{2L^2}\sqrt{\frac{Eh^2}{12\rho}} \tag{4.1}$$

where f_0 is the lowest eigenfrequency, L the span between the supports and h the height of the beam. Measurements were carried out both for a 6.2 m beam and a joined 9.3 m beam. The beam was placed on two supports, 10 cm from the ends, giving a span of 6.0 m. The joined beam was placed on three support, two supports 15 cm from the ends and a support in the middle. Due to symmetry, the 4.5 m span between the midspan support and an outer support can be viewed as a beam on two supports. Accelerometers were placed on the middle of the beams to measure the acceleration in vertical direction and the beams were excited by hitting them vertically in the middle of the span.

Figure 4.5 shows the interval of the data from the 6.2 m beam that was used for evaluating the eigenfrequency. The frequency was calculated simply by dividing the number of periods with the time.

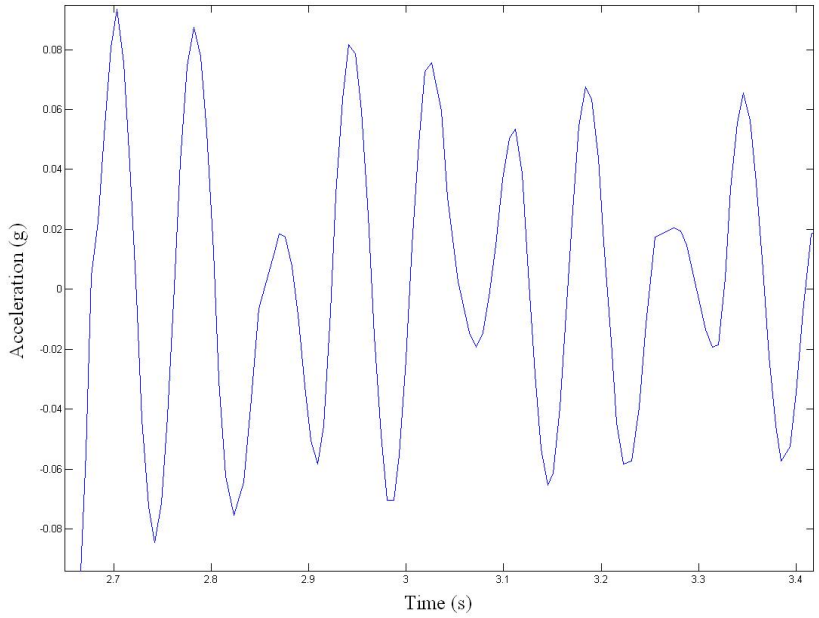

Figure 4.5: The measured oscillations of the 6.2 m beam.

The eigenfrequencies of the oscillations for both the joined and continous beam and the calculated Young's modulus for both cases are shown in Table 4.1.

	Frequency (Hz)	**Young's modulus (MPa)**
6.2 m beam	12.28	8480
9.3 m beam	21.66	8350

Table 4.1: Results from measurements on a single beam.

The Young's modulus of the joined beam was approxiamtely the same as for the continous beam. This indicates that the joint has little influence on the stiffness of the beam.

4.5. The floor without particle boards

4.5.1. Experimental setup

For the measurement on the floor without particle boards, the accelerometers were placed mainly on the supporting beams, but also on the secondary spaced boarding. Since the main objective of the measurements was to examine the eigenfrequencies below 100 Hz, the accelerometers were placed in the middle of the span between the midspan support and the outer supports, where the displacements were assumed to be large. Moreover, they were spread over all beams to examine if the whole floor behaves in a similar manner. The positioning of the accelerometers is shown in Figure 4.6 and their coordinates are given in Appendix A.

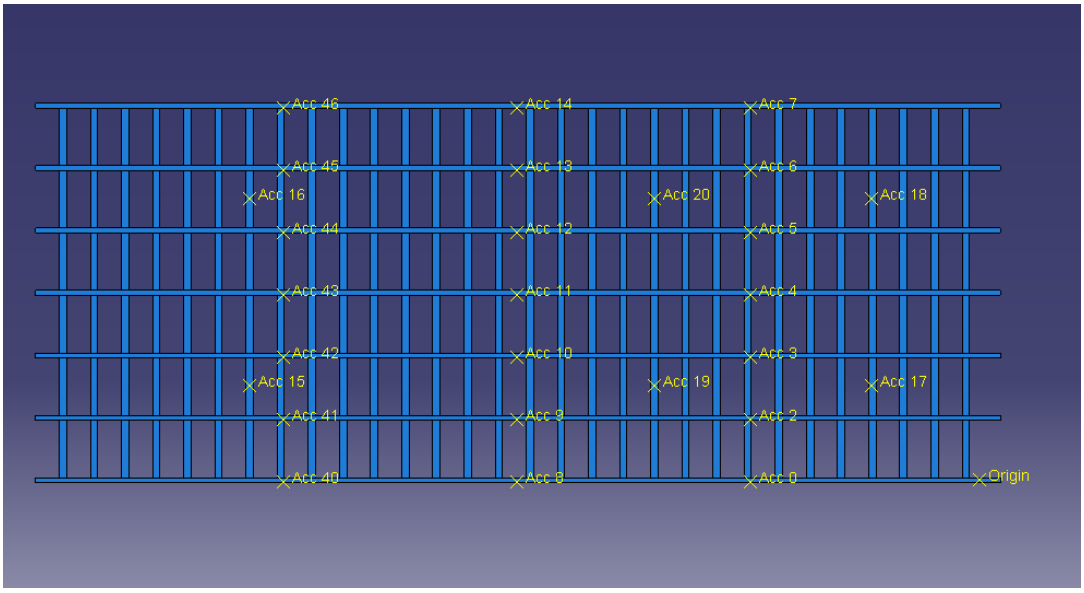

Figure 4.6: Positioning of the accelerometers for measurements on the floor without particle boards.

The accelerometers on the beams were screwed on the side of the beams except for those placed over the midspan support which were screwed on top of the beams. The accelerometers on the secondary spaced boarding were screwed to the upside of the boards.

The floor without particle boards were only measured for transient loads. The structure was struck with a rubber mallet at four different points. The excitation points were placed on four different beams and with various distances from the supports to ensure that several eigenmodes were excited. If the structure is excited at a point where one or more of the eigenmodes have a node (a point that stands still during the oscillations) those eigenmodes will not be excited. This makes it

important to excite the structure at several points and therefore the excitation points were spread out. The chosen excitation points are shown in Figure 4.7 and their coordinates are given in Appendix A.

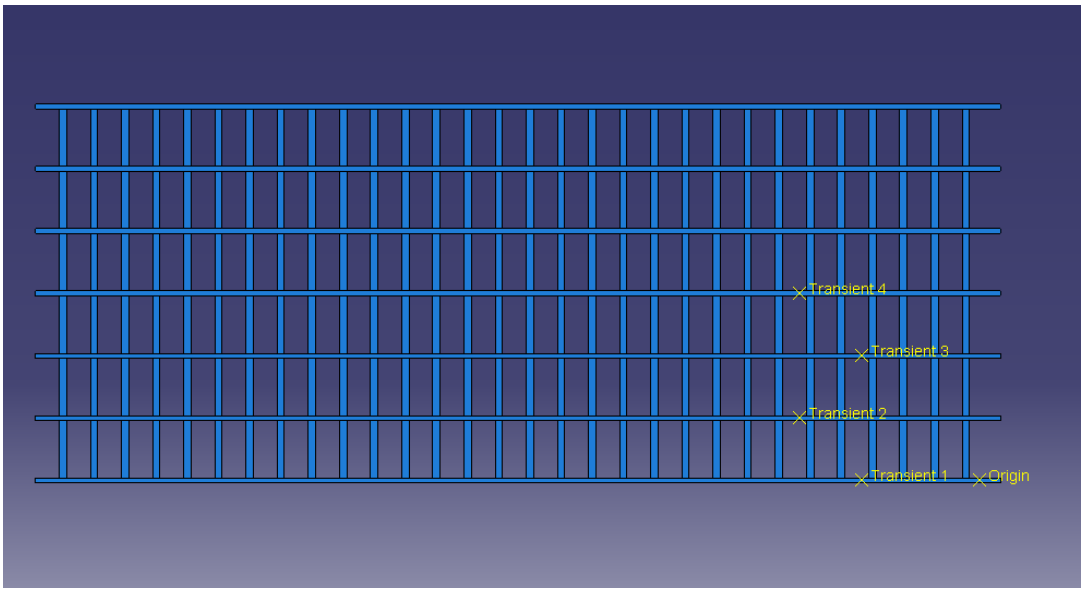

Figure 4.7: Excitation points for the floor without particle boards.

4.5.2. Analysis

Eigenfrequencies were determined for transient excitations number 1 and 4 using data from all accelerometers. Table 4.2 shows a compilation of the frequency peaks that were recurring on multiple accelerometers.

Transient 1	17.4	19.4	20.5	23.5	26.1	27.8	35.3	46.2	68.2	—
Transient 4	17.4	19.2	20.5	—	—	—	35.3	—	68.0	73.4

Table 4.2: Compilation of frequency peaks recurring on multiple accelerometers for the floor without particle boards. Frequencies are given in Hertz.

To evaluate the damping ratio, eight different signals were analysed; four from *Transient 1* and four from *Transient 4*. The exponential fitting gave an average value of $\zeta = 0.0284$.

4.6. The floor with particle boards

4.6.1. Experimental setup

For the measurements on the floor with particle boards, all accelerometers were placed on the particle boards; some over the beams and some in between the beams. A row of accelerometers were placed along one of the beams to be able to determine the deflection of the beam and another row was placed perpendicular to the beams to determine the deflection in that direction. The rest were spread out over the structure. A sketch over the accelerometer placement is shown in Figure 4.8 and their coordinates are given in Appendix A.

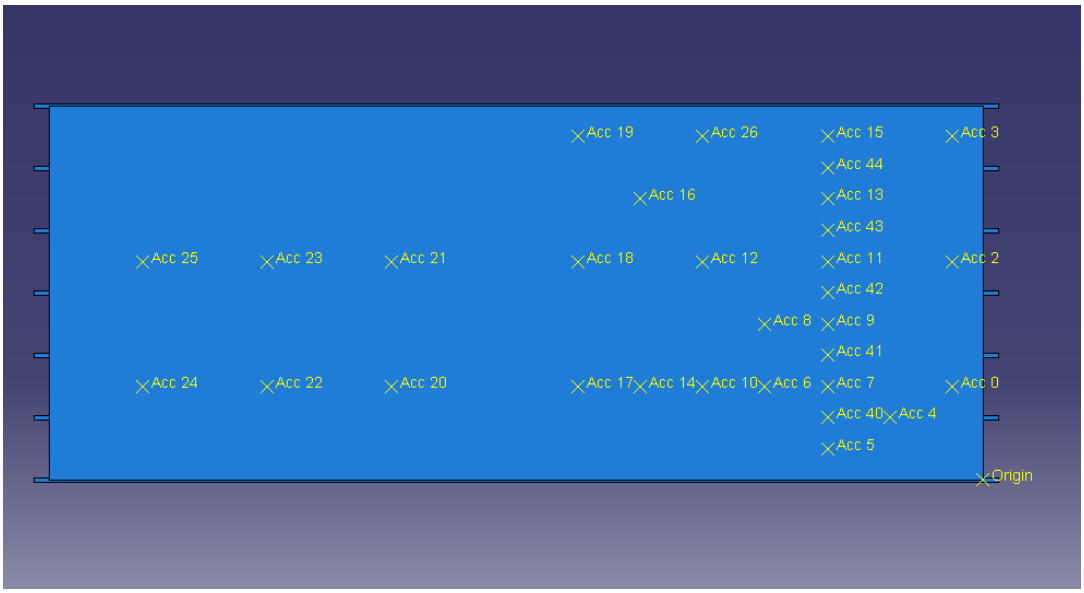

Figure 4.8: Positioning of the accelerometers for measurements on the floor.

Three harmonic loads (FS 1-3) and three transient loads (T 1-3) were applied to the floor structure with particle boards. The excitation points were chosen both on and between the beams and with different distances from the supports. The excitation points are illustrated in Figure 4.9 and their coordinates are given in Appendix A.

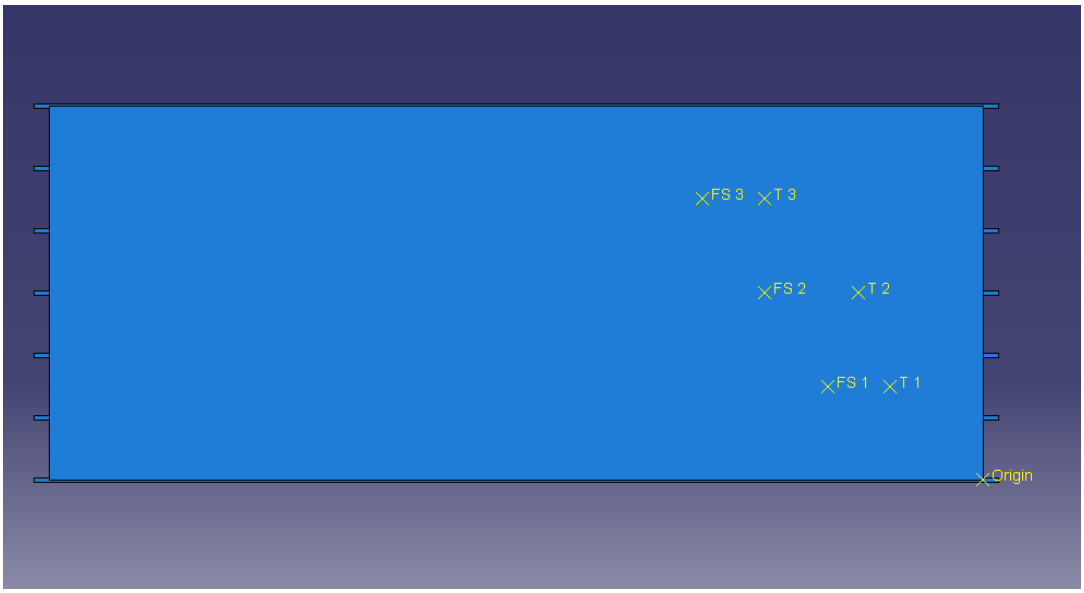

Figure 4.9: Excitation points for the floor.

4.6.2. Analysis

Two different measurements were used to analyse the eigenfrequencies of the floor with particle boards, *Frequency Sweep 2* and *Transient 2*. Frequency peaks recurring on multiple accelerometers are shown in Table 4.3.

Frequency Sweep 2	17.4	23.7	26.7	42.0	45.3	~ 69	~ 85	~ 95	—
Transient 2	16.3	23.5	41.4	44.1	68.4	~ 73	~ 77	~ 88	90-96

Table 4.3: Compilation of frequency peaks recurring on multiple accelerometers for the floor with particle boards. Frequencies are given in Hertz.

4.7. The floor-wall structure

4.7.1. Experimental setup

The same experimental setup as was used for the floor structure with particle boards was used for the complete floor-wall structure. Both the accelerometer positioning and the excitation points were the same, except for the position of accelerometer 4 in the frequency sweep. It was moved to a point with the same x-coordinate but with a y-coordinate 0.9 m (instead of 0.6 m). For the measurements with transient excitation, the position was the same as for the measurements on the floor structure.

4.7.2. Analysis

To obtain the eigenfrequencies for the complete floor-wall structure, four different measurements were used; *Frequency Sweep 1*, *Frequency Sweep 2*, *Transient 1* and *Transient 2*. Frequency peaks recurring on multiple accelerometers are shown in Table 4.4. Since some of the peaks were relatively broad, the value of the peak frequency varies a bit between the accelerometers. No decimals are therefore given, instead a rounded average value of the frequencies that were regarded to belong to the same eigenmode are shown.

Frequency Sweep 1	21	24	31	35	42	47	53	65	69	75	84	95
Frequency Sweep 2	21	25	30	41	46	69	72	87	95			
Transient 1	15	20	23	31	35	42	46	53	69	74	84	94
Transient 2	15	20	24	42	46	55	69	72				

Table 4.4: Compilation of frequency peaks recurring on multiple accelerometers for the floor-wall structure. Frequencies are given in Hertz.

Many mode shapes were extracted from the frequency sweep measurements, but only the mode shapes corresponding to the eigenfrequencies given in Table 4.4 were studied. A compilation of these mode shapes are shown in Figure 4.10 to 4.19. It has to be taken into consideration that there were relatively few accelerometers on one side of the wall. Therefore, the mode shape pictures are sometimes not able to represent the deflection in a satisfactory manner on that side of the wall.

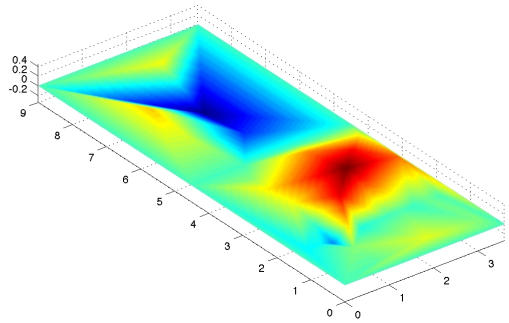

Figure 4.10: The mode shape of the floor-wall structure at 15.9 Hz.

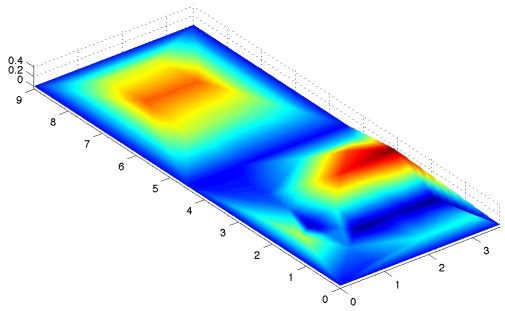

Figure 4.11: The mode shape of the floor-wall structure at 20.2 Hz.

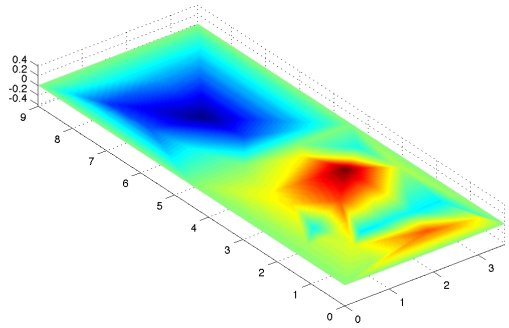

Figure 4.12: The mode shape of the floor-wall structure at 24.7 Hz.

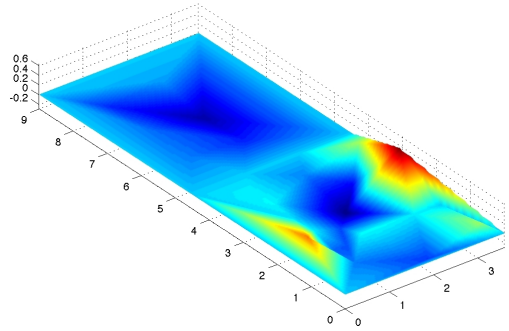

Figure 4.13: The mode shape of the floor-wall structure at 29.5 Hz.

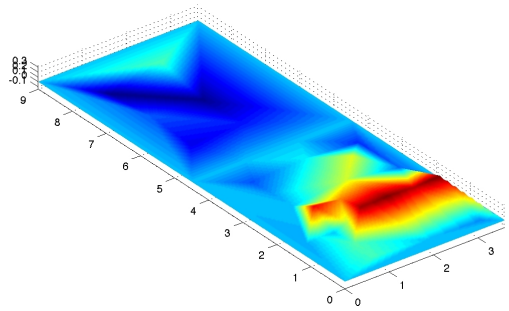

Figure 4.14: The mode shape of the floor-wall structure at 35.8 Hz.

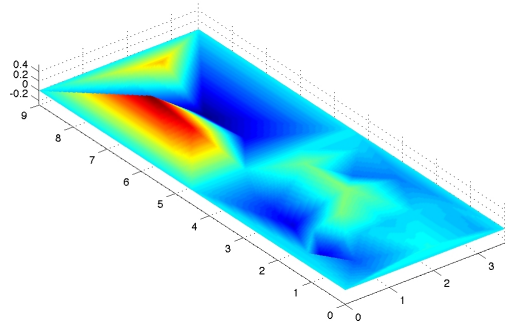

Figure 4.15: The mode shape of the floor-wall structure at 41.1 Hz.

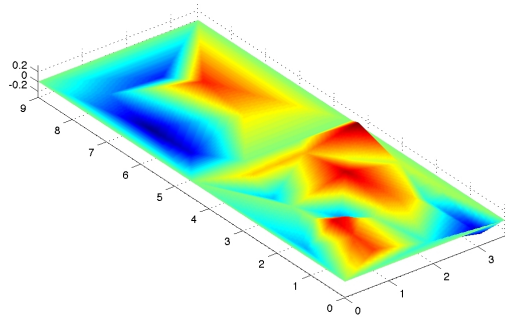

Figure 4.16: The mode shape of the floor-wall structure at 69.1 Hz.

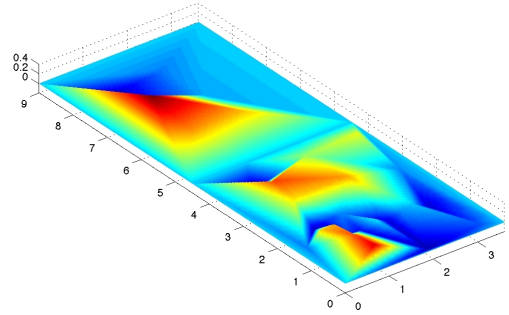

Figure 4.17: The mode shape of the floor-wall structure at 73.4 Hz.

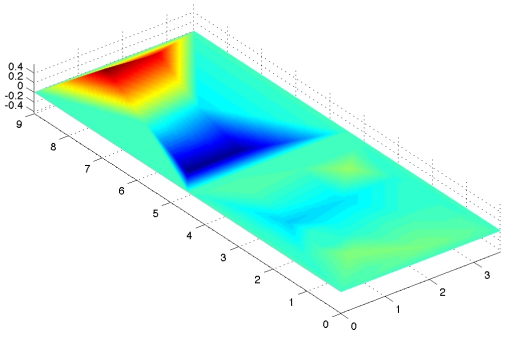

Figure 4.18: The mode shape of the floor-wall structure at 85.4 Hz.

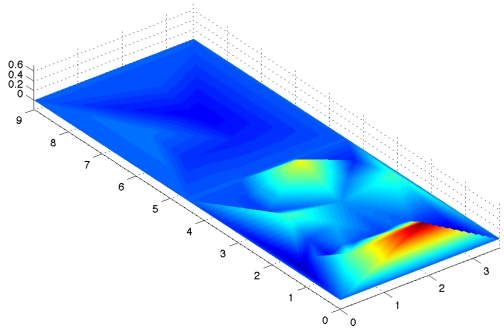

Figure 4.19: The mode shape of the floor-wall structure at 92.3 Hz.

5. Finite Element Modeling

5.1. Introduction to the finite element method

When you are dealing with engineering mechanics or encounter various physical problems in other areas of work, the problems are generally modeled as differential equations. Most of the times this results in a differential equation or system of differential equations that is too complicated to be solved by classical analytic methods. The finite element method is a way to derive an approximate solution to general differential equations by numerical means [3].

Physical problems may be described in one-, two- or three-dimensional regions with a differential equation or equations. Although the sought variable varies over the region in a complex non-linear manner the finite element method can find an approximative solution by dividing the region in elements in which the variable can be assumed to vary in a certain fashion. The approximation over an element is usually made by a polynomial and can be linear, quadratic, cubic, etc. The collection of elements in a region is called a finite element mesh. The behavior of each element can be determined by the use of the selected approximation. A solution for the behavior of the entire region can then be obtained by assembling all elements into a global linear equation system.

When you derive a finite element formulation of a problem you transform a continuous system with an infinite number of unknowns, i.e. degrees of freedom, to a discrete system with a finite number of unknowns. Problems that are solved by the finite element method often contains thousands of degrees of freedom and can only be solved by computers. By creating a finer mesh a more accurate solution is obtained, but at the cost of an increased computation time.

5.2. Abaqus

There are numerous software applications for finite element analysis and computer-aided engineering. Some of the most well known commercial softwares are: Ansys, Nastran, Comsol, LS-Dyna and Abaqus. The finite element modeling and calculations in this master's dissertation are performed in Abaqus because of the friendly user interface and the availability at Lund University.

Abaqus consists of four main software products: Abaqus\CAE, Abaqus\Standard,

Abaqus\Explicit and Abaqus\CFD. Abaqus\CAE is a customizable user interface used for designing, modeling, pre- and post-processing and visualizing the finite element analysis result. Abaqus\Standard is a general-purpose implicit integration solver ideal for static and low-speed dynamic events. Abaqus\Explicit is another solver that use an explicit integration method to solve for example high-speed, highly nonlinear and transient response events. Abaqus\CFD is a new application for Abaqus 6.10 which provides advanced computational fluid dynamics capabilities.[11]

The software applications used in this project was Abaqus\CAE to create the model and view the results and Abaqus\Standard to perform all finite element analyses. Abaqus 6.10 is currently the most recent version of Abaqus but in this case Abaqus 6.9 was used.

5.3. Materials

The structure was only exposed to small loads and displacements. This meant that non-linear materlial and geometric behavior could be neglected and allowed the materials to be modeled as linear elastic materials. The material parameters and their corresponding units are shown in Table 5.1.

Young's modulus of elasticity	E	MPa
Shear modulus	G	MPa
Poisson's ratio	ν	Dimensionless
Mass density	ρ	kg/m^3

Table 5.1: Material properties and units.

5.3.1. Construction wood

All the parts of the construction that consists of wood was modeled in the same way for the sake of simplicity. The material properties were compiled from the evaluations of the measurements of a single beam and according to characteristic properties of construction wood in construction class K24. Wood is an orthotropic material with different material properties in three different directions perpendicular. It was modeled in Abaqus as an elastic material with engineering constants according to Table 5.2. Direction 1 is aligned with the fiber direction and direction 2 and 3 are perpendicular to the fiber direction. For simplicity, the properties in the two perpendicular directions was assumed to be equal.

E_1	E_2	E_3	G_{12}	G_{13}	G_{23}	ν_{12}	ν_{13}	ν_{23}	ρ
8500	350	350	700	700	50	0.2	0.2	0.3	432

Table 5.2: Material parameters for construction wood [4, 13].

5.3.2. Particle board

The particle board that constitute the floor surface is a transversal isotropic material but was regarded as an isotropic material with properties according to Table 5.3.

E	ν	ρ
3000	0.3	767

Table 5.3: Material parameters for the particle boards [4, 13].

5.3.3. Plaster board

The plaster boards make up the visual part of the wall that separates the rooms in the acoustic laboratory. They are modeled as an isotropic material with properties according to Table 5.4.

E	ν	ρ
2000	0.2	692.3

Table 5.4: Material parameters for the plaster boards [12].

5.4. Damping

Damping was included in the model to prevent the structure from oscillating infinitely in time when applying a transient load and thus enable an analysis of the responding behavior. The damping was modeled as Rayleigh damping in all materials and the coefficients were determined in the analyses of the experimental data for the floor structure without particle boards. The damping ratio was determined to 2.84% which gave the coefficents $a_0 = 4.44$ and $a_1 = 0.000159$ when using the first and second measured eigenfrequencies (19.2 Hz and 35.4 Hz) of the floor structure without particle boards. These damping coefficents were used in all the models even though the damping was increased in the structure when the floor boarding and the wall was added. This simplification is neglectable since the influence of damping is not very significant when performing a modal analysis if the damping ratio is low.

5.5. Analysis procedures

Three different analyses were performed on the models; modal, steady state and transient analysis.

The modal analysis determines the eigenvalues (eigenfrequencies) and eigenvectors (mode shapes) of the model. It was only performed on a single beam. The analysis was limited to frequencies in the range 0-100 Hz.

The transient analysis uses an implicit solver to determine the response of the structure when excited by a pulse load. The pulse load was modeled as a concentrated force with a maximum amplitude of 100 N in vertical direction. The amplitude of the pulse ramps up from zero to maximum amplitude in 0.01 s and down from maximum amplitude to zero in 0.01 s using two third degree polynomials [5].

The steady-state analyses was performed to imitate the frequency sweep measurements. The analyses were performed for a discrete number of frequencies studying the interval 5-100 Hz with a solution determined at every 0.25 Hz. The harmonic load was modeled as a concentrated force with an amplitude of 100 N.

5.6. Analysis of a single beam

The intention of performing calculations on a single beam was to verify the lowest eigenfrequencies of the analysis model for the chosen material properties and boundary conditions. It was also done to establish an appropriate mesh size that provides good results without consuming too much computing power. This was very important because a large model, as the complete floor-wall structure, may contain too many degrees of freedom if the mesh size is not chosen carefully. A too fine mesh will cause an unacceptable long computation time.

The 9.3 m long joined floor beams were modeled as continous homogeneous solids without consideration to the joints. Boundary conditions were applied where the supports were placed in the real construction. The boundary conditions over the outer supports were defined as prevented displacements in global x- and z-direction, i.e. the lateral and vertical motion of the beam was prescribed as zero at the nodes that correspond to the location of the supports. The midspan support was modeled as simply supported (pinned), which means that the displacements were prevented in all directions. If all the supports are pinned it results in a model that is much stiffer than the construction is in reality. But by allowing the outer supports to move in the lengthwise direction of the beam a more realistic stiffness is obtained.

Two different types of elements were used and evaluated in the calculations. A linear 8-node brick element and a quadratic 20-node brick element, both with reduced integration. The number of elements was chosen either by an approximate element size or an assigned number of elements to the edges of the beam. The meshes defined by an approximate element size are chosen to contain a lot more degrees of freedoms than the meshes with an assigned number of elements along the edges. In Table 5.5 the number of elements are given for the length (l), width (w) and height (h) of the beam. The results of a modal analysis between 0 and 100 Hz for different mesh sizes and element types are displayed in Table 5.5. Additional analyses with other mesh sizes were performed but only a selection of the substantial results are presented here. The mode shapes dominated by vertical displacement are highlighted with a boldface font in the table.

Element type	Linear	Linear	Linear	Quad	Quad	Quad
Element size	0.005	0.01	—	0.008	—	—
Number of elements (l×w×h)	—	—	124×4×6	—	62×1×3	62×2×3
Frequency [Hz]	4.79	4.76	4.62	4.98	5.55	5.54
	6.34	6.32	6.37	6.56	6.80	6.79
	17.44	17.30	17.11	17.93	19.03	19.01
	17.80	18.04	19.16	19.26	21.03	20.97
	21.30	**21.29**	**21.03**	**21.33**	**21.37**	**21.37**
	21.50	21.66	22.30	23.38	30.12	29.83
	29.99	30.27	31.22	**32.07**	**32.49**	**32.48**
	31.76	**31.84**	**31.72**	32.51	38.08	37.88
	42.07	41.60	41.44	42.85	45.57	45.35
	43.58	43.61	45.17	45.72	48.04	47.90
	48.34	47.85	48.68	59.34	56.15	55.72
	63.97	63.35	64.95	65.16	68.23	67.98
	76.76	75.93	76.82	78.22	**80.01**	**80.01**
	78.33	77.83	**77.52**	**79.24**	83.48	83.00
	78.58	**78.71**	80.81	80.28	86.05	85.60
	86.41	85.34	86.38	87.25	89.67	89.25
	90.38	**91.27**	**92.66**	**93.24**	**97.13**	**97.13**

Table 5.5: Eigenfrequencies for a single beam.

The final floor-wall structure has a large torsional rigidity due to the secondary spaced boarding and the floor boarding. This property and the fact that the floor-wall structure will mainly be excited by vertical loads makes the mode shapes with displacement mainly in the vertical direction crucial in this study. The vertical oscillations are also assumed to create most of the disturbing noises and vibrations that can occur in lightweight structures.

When the number of elements approaches infinity the solution converges to the analytic solution. The calculations with really fine meshes were regarded as the desired results when comparing meshes with less number of elements. The experimentally measured eigenfrequency in the vertical direction of a single beam is 21.66 Hz, which corresponds well to all calculated values. As seen in Table 5.5 the first couple of important eigenfrequencies are consistent and significant differences does not appear until the fourth eigenfrequency in the vertical direction, at roughly 90 Hz. Quadratic elements have a tendency to create a model stiffer than reality, which can be seen in the results for the fourth eigenfrequency, which clearly deviates from the key so-

lution. Quadratic elements also cause long computation times and were therefore disregarded as element type for the complete structure. The mesh with linear elements and a $124 \times 6 \times 4$ seed resulted in a solution that is in close agreement and demanded a short computation time. It also produced conveniently placed nodes which made it easy to extract data from the correct points where the accelerometers were placed on the real construction. This mesh was therefore selected to be used for the beams in the more complex models of the structure. The mesh is shown in Figure 5.1.

5.7. The floor without particle boards

The floor structure without particle boards was the first composed model analysed in the project. The main objective with this model was to determine the first eigenfrequencies of the structure, with a reasonable computation time. Only the vertical displacement of the structure was analysed in this project. The complexity of the structure made it impossible to analyse in the same way as for a single beam. Instead, other analysis methods had to be used in order to determine the eigenfrequencies of the floor structure without particle boards. A transient and a steady-state analysis were made with the loads applied at the center beam, at the same position as *Transient 4* in the experiment. The position of the loads is shown in Figure 4.7 and the exact coordinates are presented in Appendix A. Data was extracted from the nodes that correspond to the accelerometer positioning in the measurements. The eigenfrequencies from the transient analysis were determined by studying the frequency content that was obtained from an FFT-analysis of the acceleration data. To determine the eigenfrequencies from the steady-state analysis, the acceleration response of a node was plotted versus the frequency. The peaks of the curve indicates a resonance frequency of the structure.

The boundary conditions were defined in the same way as for the single beam and were applied on all the beams in the structure. The mesh of the beam that was established in Section 5.6 was used in the model of the floor structure as well. The seed of the secondary spaced boarding was made with the experience from the analysis of a single beam in mind. The element size in the longitudinal direction of the boards was the same as for a beam, i.e. 7.5 cm, which resulted in 48 elements along the board. The height of the board was divided into three elements and the width into two elements. A part of the mesh is shown in Figure 5.1.

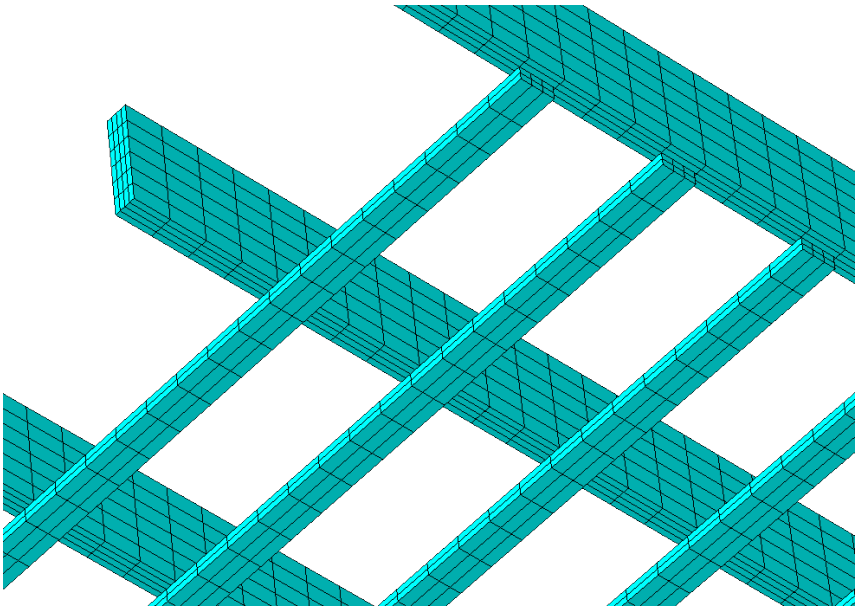

Figure 5.1: Part of the mesh of the floor structure without particle boards.

The floor structure without particle boards consists of seven load-bearing beams and an underlaying layer of secondary spaced boarding. The most difficult challenge when creating a model of an assembled structure is to create proper constraints at the connections between the parts. These connections determine most of the the torsional stiffness, hence the behavior of the whole structure, and are therefore important in order to get a realistic result. If the meshes of the parts are relatively sparse the connecting surfaces may only include a few nodes. It can then be important which surface that is set as master or slave surface when using the *Tie* constraint in Abaqus that fully constrain surfaces. All nodes on the slave surface will strictly follow the displacement of the master surface. This fact is substantial when connecting the beams and the secondary spaced boarding. Since the connecting surfaces of the boards only have one node in the direction of the width of the beams, and the beams have five nodes, the surface of the secondary spaced boarding must be set as master to gain torsional stiffness between the parts. Another solution is to create sections on both parts that can be used as surfaces for the tie constraint. However, this alternative causes a high complexity of the mesh.

A tie constraint with the beams as slave surface was regarded as the best alternative for this model and the other more complex models. To validate our choice, two additional models were analysed. One with a tie constraint and the beams as master surfaces, and one with sections on both parts which created smaller surfaces for the tie constraint. As expected, the first model showed too much rotational displacement of the beams due to the lack of torsional stiffness. The results from the second model were of good resemblance to the results from the chosen model, even though there was a big difference between the meshes. But the computation time for this model

was several times longer which made it unsuitable for both this structure and more complex structures. Our conclusion was that the model with the beams as slave surfaces and a tie to the secondary spaced boarding over the total area of contact was preferred to continue working with. A compilation of the results from different accelerometer positions are shown in Table 5.6.

Steady-state analysis	17.4	18.4	20.4	26.0	27.2	29.0	31.3	33.0	43.5
	53.0	57.0	61.3	73.0	83.0	96.0			
Transient analysis	17.6	19.1	25.4	26.6	29.7	36.5	44.1	46.9	

Table 5.6: Eigenfrequencies (Hz) for the floor structure without particle boards.

A compilation of the approximated eigenfrequencies from the measurements and the calculations that correspond well to each other is shown in Table 5.7. The first eigenfrequency from the model appeared at the exact same frequency as for the measurements and similarity to the measured results can also be seen for the higher eigenfrequencies. Mode shapes were not evaluated from the measurement data, hence no mode shape comparison was made. The resemblance between the eigenfrequencies of the model and the real structure was concidered as a good enough result to move on to the floor model with particle boards.

Calculated results	17	19	20	27	29	33	44	73
Measurement results	17	19	21	26	28	35	46	68

Table 5.7: Comparison of the eigenfrequencies (Hz) for the floor structure without particle boards.

5.8. The floor with particle boards

To create the floor structure with particle boards a new part was added to the model. In the real construction, the floor surface was assembled by particle boards that were glued and screwed to the beams and also glued at the seam. By gluing them together, the interaction between the boards is increased, and the floor surface may therefore be regarded as a single plate. The floor was created as one part with the material properties of particle board, see Table 5.3. It was meshed with two elements along the thickness of the plate and the surface was made up by 7.5×7.5 cm^2 square elements. As for the rest of the structure, 8-node linear elements were used. A picture of the mesh is shown in Figure 5.2

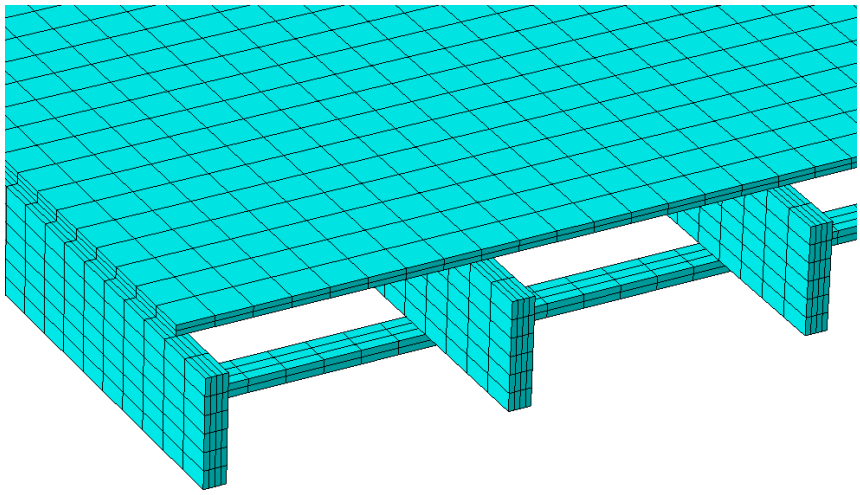

Figure 5.2: The mesh of the floor structure with particle boards.

Both transient and steady-state analyses were carried out on the floor with particle boards. The loads were placed on the middle beam at the same positions as *Transient 2* and *Frequency Sweep 2*, as shown in Figure 4.9. The exact coordinates are found in Appendix A. The boundary conditions were defined in the same way as for the model without floor boarding. The connections between the floor surface and the underlaying beams were created as a tie constraint with the beams as slave surfaces, just like the connection between the secondary spaced boarding and the beams. The analyses of the data from the transient and the steady-state analyses gave the eigenfrequencies of the structure presented in Table 5.8. The data from nodes at a number of selected accelerometer positions, placed both on the beams and in the spans between the beams, were used when evaluating the eigenfrequencies of the structure. The eigenfrequencies given in the table were recurrent for multiple nodes.

Steady-state analysis	15.5	16.5	22.3	23.6	27.6	29.6	31.6	43.9
	47.6	59.6	∼64	∼88	∼97			
Transient analysis	15.6	17.2	21.9	23.1	26.2*	28.5*	30.5	33.2
	39.1	43.4	46.9	51-57**	61.7-65.2**			

Table 5.8: Eigenfrequencies (Hz) for the floor structure with particle boards.

* Eigenfrequencies that only occur on the beams.
** Eigenfrequencies that only occur on the floor in the spans between the beams.

When compared to the results from the measurements which are presented in Table 4.3, several eigenfrequencies are found to coincide. Table 5.9 shows a compilation of

approximated eigenfrequencies extracted from the measurements and the calculated results that correspond well to each other. The first eigenfrequency from the model appeared at the exact same frequency as for the measurements and similarity to the measured results can also be seen for the higher eigenfrequencies. Mode shapes were not evaluated from the measurement data, hence no mode shape comparison was made. The resemblance between the eigenfrequencies of the model and the real structure was concidered as a good enough result to proceed to the modeling of the complete floor-wall structure.

Calculated results	17	24	28	44	48	64	88	97
Measurement results	17	24	27	42	45	69	85	95

Table 5.9: Comparison of the eigenfrequencies (Hz) for the floor structure with particle boards.

5.9. The floor-wall structure

The final structure was completed by adding a wall to the floor structure with particle boards. The wall was modeled as it is built in reality, with plasterboards attached to the horizontal and vertical wall-beams. The joist, top plate and the vertical beams was given the same material properties as the floor beams. In the real construction, the top plate and the outer vertical beams are glued and screwed to the surrounding concrete wall which creates a firm connection. The boundary conditions along these edges are therefore assumed to be prevented displacement in all directions. Thus also constraining the rotations at the wall boundaries. All connections between the instances were created as tie constraints with the slave surface chosen to create as rigid coupling as possible. It is especially important that the floor surface is set as master in the connection to the joist since it has less nodes along the connecting surface. The beams were meshed with 4 elements in width, 5 element in hight and approximately 7.5 cm long elements in the lengthwise direction. The plasterboards were meshed in the same manner as the floor board described in Section 5.8. The material properties of the plasterboards are displayed in Table 5.4. The insulation which fills the gaps between the beams in the built construction was disregarded in this model since it is assumed to not influence the vibrations of the structure.

Two transient and two steady-state analyses were performed on the floor-wall model. The loads corresponded to *Transient* 1 and 2, and *Frequency Sweep* 1 and 2 of the measurements. The excitation points are shown in Figure 4.9 and the coordinates are presented in Appendix A. The eigenfrequencies determined from the results of the analyses are presented in Table 5.10, showing frequencies recurring on multiple accelerometer positions. A comparison to the measured results will follow in Section 6. Ten different accelerometer positions were studied in the analyses of both calculated and measured data. The graphic results from the steady-state analy-

ses in Abaqus were also used to evaluate whether the structure is oscillating at an eigenfrequency.

Steady-state	15.8	16.8	18.6	22.9	23.9	25.1	34.9	38.4	43.7	46.0
analysis 1	48.2	50.0	54.0	59.6	67.8	71.4	74.1	81.2	97.7	
Steady-state	15.9	16.6	22.7	23.9	27.5	29.0	32.3	43.6	48.6	58.7
analysis 2	65.3	86.9								
Transient 1	16.0	17.6	22.3	23.4	31.3	34.0	∼39	43.4	47.3	55-58
	∼71									
Transient 2	15.6	17.6	22.3	23.4	26.6	30.9	33.6	40.6	43.4	∼ 48
	∼ 50									

Table 5.10: Eigenfrequencies (Hz) for the floor-wall structure.

The results from *Transient 1* and *Steady-state analysis 1* differ slightly from *Transient 2* and *Steady-state analysis 2* due to the acentric excitation point positioning, thus exciting other eigenfrequencies. The mode shapes which correspond to the eigenfrequencies extracted from Steady-state analysis 2 are displayed visually in Figure 5.3-5.14. The mode shapes are printed from the graphical interface in Abaqus. A comparison to the mode shapes created from the experimental data is made in Section 6.

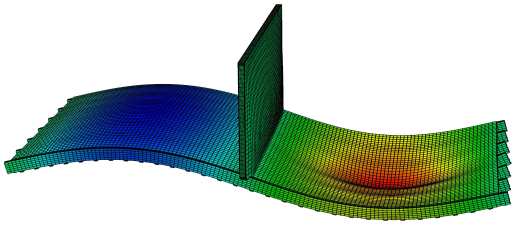

Figure 5.3: Mode 1 at 15.9 Hz.

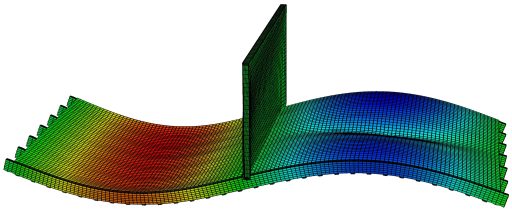

Figure 5.4: Mode 2 at 16.6 Hz.

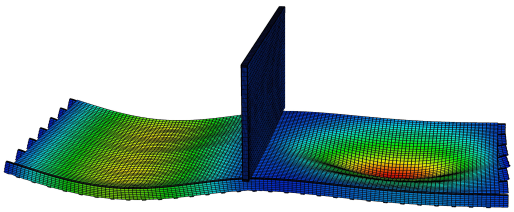

Figure 5.5: Mode 3 at 22.7 Hz.

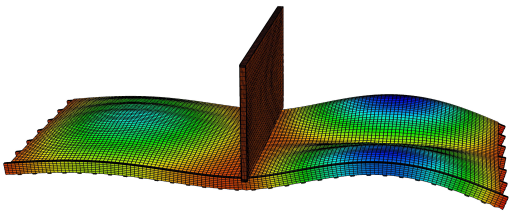

Figure 5.6: Mode 4 at 23.7 Hz.

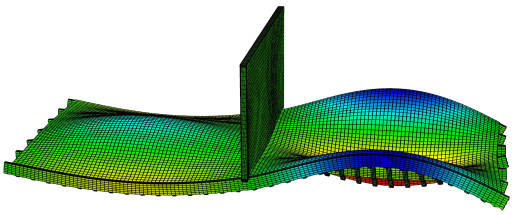

Figure 5.7: Mode 5 at 27.5 Hz.

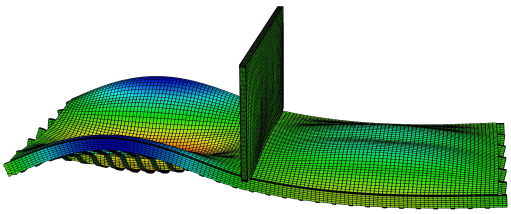

Figure 5.8: Mode 6 at 29.0 Hz.

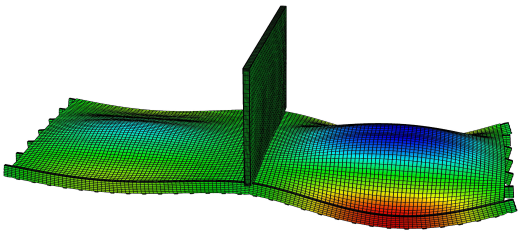

Figure 5.9: Mode 7 at 32.3 Hz.

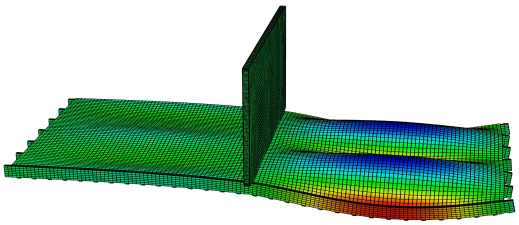

Figure 5.10: Mode 8 at 43.6 Hz.

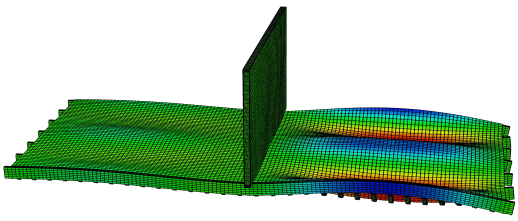

Figure 5.11: Mode 9 at 48.6 Hz.

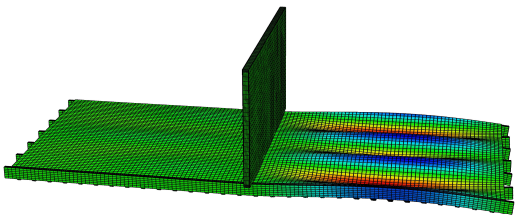

Figure 5.12: Mode 10 at 58.7 Hz.

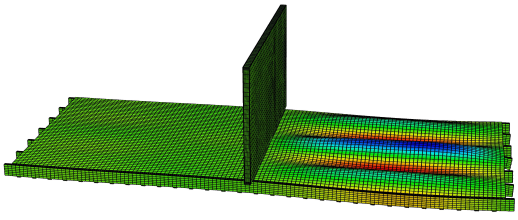

Figure 5.13: Mode 11 at 65.3 Hz.

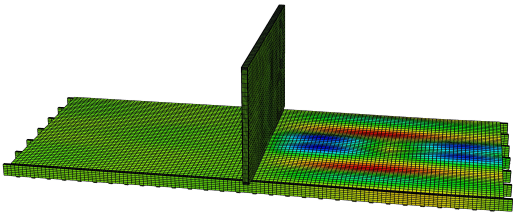

Figure 5.14: Mode 12 at 86.9 Hz.

6. Results and Discussion

6.1. Introduction

In this chapter, the objective is to summarise the results of the measurements and the simulations of the complete floor-wall structure and to compare the results. The measurement and simulation results of the simpler structures were used to simplify the modeling of the complete structure and will not be evaluated further than what was done in the previous chapters. The resemblance of the eigenfrequencies from the measurements and the simulations will be analysed. To establish that the eigenfrequencies from the measurements and from the model are actually from a similar eigenmode, a comparison of the mode shapes corresponding to those eigenfrequencies will be carried out.

6.2. Eigenfrequencies

The eigenfrequencies found from the measurement data are shown in Table 4.4 and the eigenfrequencies from the model are shown in Table 5.10. The frequencies presented in the tables are compiled in Table 6.1. The frequencies assumed to be from the same eigenmode are paired together in the table.

Measurements	15	—	21	24	—	31	35	—	42	46	53
Simulations	16	17	23	24	27	31	34	39	44	48	58
Measurements	69	74	85	95							
Simulations	66	71	84	—							

Table 6.1: Approximate eigenfrequencies (Hz) from both measurements and simulations.

From the data in Table 6.1 a lot of similarities are found between the eigenfrequencies from the measurements and the simulations. The first frequency at approximately 15 Hz from the measurements seems to be reproduced with very good precision in the model where two eigenfrequencies appeared at 16 and 17 Hz (the two numerical eigenmodes have similar mode shapes, see Figure 5.3 and 5.4). Even though the result seems satisfactory, good resemblance in eigenfrequencies is not proof enough that the dynamic behavior of the structure has been reproduced by the model. To be sure that the model behaves in accordance to the real structure, not only the eigenfrequencies must be similar, but also the mode shapes.

6.3. Mode shapes

To establish the similarity between mode shapes, two comparison methods were employed. The first method was to simply compare the plots visually. The other method is more complicated and was developed to determine a comparative number to describe the resemblance of two mode shapes. The method is based on the scalar product of two vectors. A mode vector is obtained by extracting the displacements at a single moment in time during an oscillation at an eigenfrequency. Two mode vectors are compared by normalising them and calculating the absolute value of the scalar product. If the result is equal to 1, the mode shapes are identical. If the result is equal to 0, the mode vectors are orthogonal (i.e. completely different).

To be able to use the scalar vector method, the mode shape vectors must first be extracted from the measurement and the simulation data. The accelerations in the frequency sweep signals from the measurements are very noisy and mode vectors can not be extracted directly. Instead, the accelerations are integrated twice resulting in smoother displacement signals. An example of an acceleration signal integrated to velocity and displacement is shown in Figure 6.1. The average value has been subtracted from the acceleration signal, but it is evident from the figure that there is a large drift in the signal which dominates the oscillations for the velocity and the displacement.

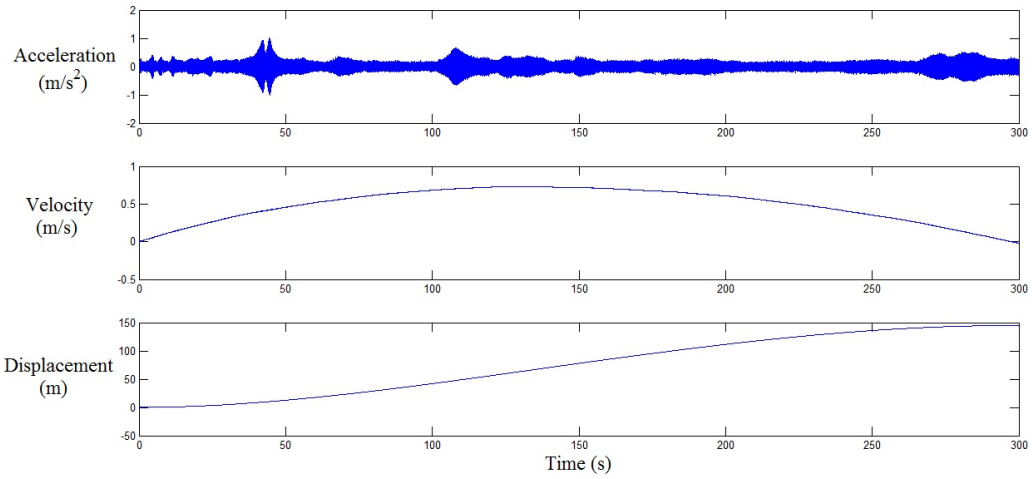

Figure 6.1: Measured accelerations integrated to velocity and displacement.

Intervals of the raw acceleration signals where the structure is oscillating with an eigenfrequency were extracted manually by identifying the determined eigenfrequencies from the RMS-plots in the raw signal. An eigenfrequency at 15.6 Hz was discovered in the beginning of the raw signal, which was impossible to identify in the RMS-plot due to the resolution. The eigenfrequencies identified in the raw accel-

eration signals used for extracting the mode shapes are given in Table 6.2. Only *Frequency Sweep 2*, with excitation point over the middle beam, was used to evaluate the mode shapes.

15.6	21.1	24.5	29.8	41.7	46.5	68.8	72.1	94.3

Table 6.2: Eigenfrequencies (Hz) from the raw acceleration signals.

Since the structure was vibrating, it was known that the displacements oscillated around zero. For all eigenfrequencies, an interval containing two oscillation periods was extracted. A second degree polynomial was fitted to the displacement interval to describe the integrated drift. The integrated drift was then subtracted from the displacement which resulted in a signal oscillating around zero. An example is illustrated in Figure 6.2. The mode vector was extracted by searching for the sample where the sum of the displacements in all 31 accelerometers was maximal and assembling all the displacements from that sample into a vector.

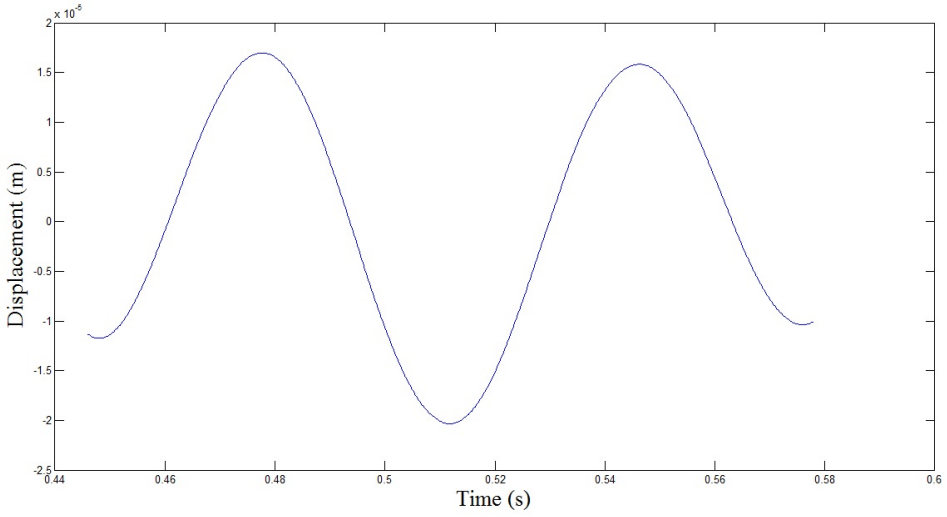

Figure 6.2: Displacement from integrated measured accelerations, with integrated drift subtracted.

The mode vectors from the model were created by extracting the displacements from the nodes at coordinates corresponding to the accelerometer positions. These were assembled into mode shape vectors in the same order as the mode vectors from the measurement data. The frequencies at which the mode vectors were extracted are given by *Steady-state Analysis 2* in Table 5.10.

The mode vectors were normalised and all vectors from measurements were multiplied with all vectors from the model to determine the comparative number. The result is shown in Table 6.3. The top three matches for all eigenfrequencies from the

model are given, as long as the result is larger than 0.5. The most significant results, the results with good resemblance of modes expected to be similar, are presented with a bold font. As expected, there is a good resemblance between the measured eigenmode at 15.6 Hz and the eigenmodes at 15.9 and 16.6 Hz from the model. For the 29.0 Hz eigenmode in simulations, there is actually a better result when compared to 15.6 Hz than 24.5 Hz. It could be explained by the fact that the mode shape of the eigenmode at 29.0 Hz in the model is similar to the first eigenmode at the accelerometer locations. The largest difference to the eigenmode at 15.6 Hz is at the outer beams (which can be seen in Figure 6.3 and 6.7 in the visual comparison below) where there are no accelerometers. Generally, the best results were obtained for the frequencies paired together in the eigenfrequency section above.

Eigenfrequencies (Hz)		Comparative
Simulations	**Measurements**	**number**
15.9	15.6	**0.83**
	24.5	0.56
16.6	15.6	**0.94**
	24.5	0.60
22.7	21.1	**0.76**
23.9	21.1	**0.92**
	41.7	0.55
	46.5	0.52
27.5	24.5	0.54
	46.5	0.52
29.0	15.6	0.71
	24.5	**0.68**
32.3	29.8	0.55
43.6	41.7	**0.68**
	15.6	0.65
	46.5	0.64
48.6	46.5	**0.78**
	41.7	0.67
58.0	68.8	0.54
	72.1	0.51
65.5	68.8	0.60
	72.1	0.60
86.9	72.1	0.58
	46.5	0.56
	68.8	0.55

Table 6.3: Results of the comparison of mode shapes from simulations and measurements.

The mode shapes were also compared visually by studying the mode plots from the *Measurements* and the *Finite Element Modeling* chapters. The most similar mode shapes are presented in Figure 6.3 to 6.14. It should be kept in mind that the mode shapes from the measurements used all three frequency sweep excitations to create the mode plots while the model mode plots are the results from *Steady-state analysis 2* only.

The mode shapes of the first eigenmode from simulations and measurements are shown in Figure 6.3 and 6.4. There is an obvious resemblance, the floor oscillates with the shape of a sinusoidal wave along the beams in both cases. In the measured mode shape, it is a little less evident, but the two sides of the floor are mainly oscillating in antiphase.

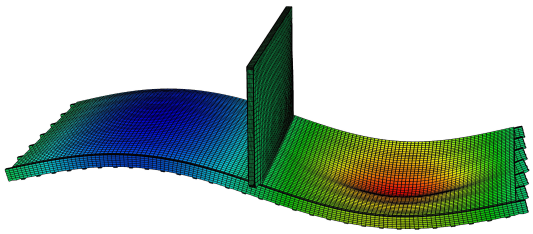

Figure 6.3: Mode shape at 15,9 Hz from simulations.

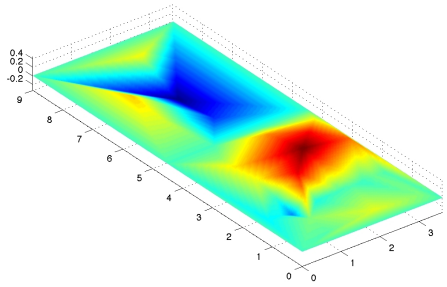

Figure 6.4: Mode shape at 15,9 Hz from measurements.

Figure 6.5 and 6.6 shows the eigenmodes with frequencies just over 20 Hz. These are probably the mode shapes with the most striking resemblance. Both sides of the wall are oscillating in phase with the shape of half a wavelength along the beams for both simulations and measurements.

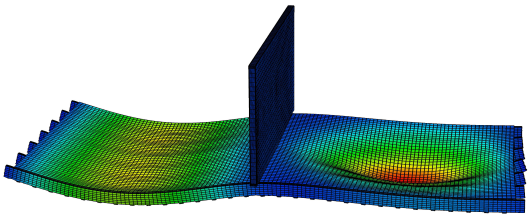

Figure 6.5: Mode shape at 22.7 Hz from simulations.

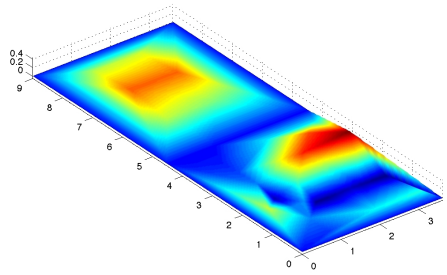

Figure 6.6: Mode shape at 20.2 Hz from measurements.

In Figure 6.7 and 6.8, the 29.0 Hz eigenmode from the model is compared to the eigenmode at ∼24.5 Hz from measurements. Along the middle beams of both cases, the floor is oscillating with the shape of a sinusoidal wave. The difference is the inflection of the outer beam, which has a large amplitude for the model. This is not seen in the simulations, but could be explained by the fact that there are almost no accelerometers at the outer beams, especially on the left side of the wall in the plots.

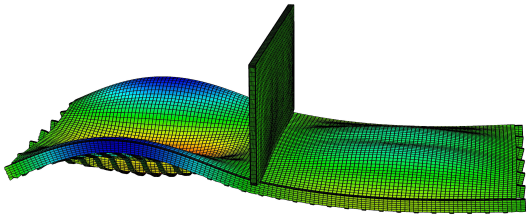

Figure 6.7: Mode shape at 29.0 Hz from simulations.

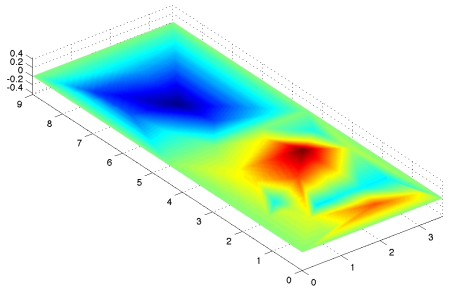

Figure 6.8: Mode shape at 24.7 Hz from measurements.

Figure 6.9 and 6.10 shows the eigenmode at 32.3 Hz from the model and the measured eigenmode at ∼30 Hz. For both measurements and simulations, both sides of the wall oscillates in phase with the shape of half a wavelength along the middle beams. In the model, the outer beams have the same deflection but in antiphase compared to the middle beams. This is obvious also for the measured mode shape, but not quite as evident at the utmost beams due to the lack of accelerometers.

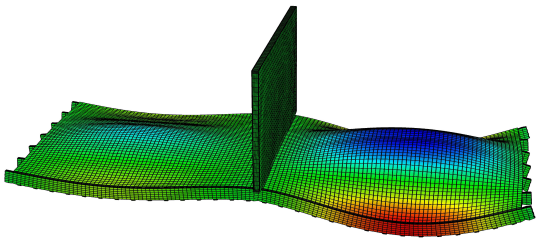

Figure 6.9: Mode shape at 32.3 Hz from simulations.

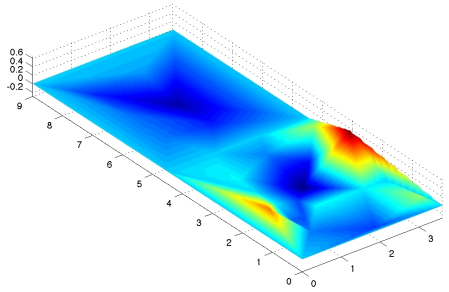

Figure 6.10: Mode shape at 29.5 Hz from measurements.

The mode shapes of the eigenmodes at 48.6 Hz from the model and ∼46 Hz from measurements are shown in Figure 6.11 and 6.11. For higher frequencies, the mode shapes in general become more complex. The deflection of the model eigenmode is probably too complex to be caught by just 32 accelerometers, although some resemblance can be seen. For example, there is a wave pattern perpendicular to the beams in both cases, but the number of wavelengths does not match.

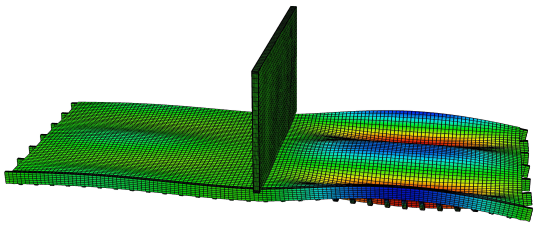

Figure 6.11: Mode shape at 48.6 Hz from simulations.

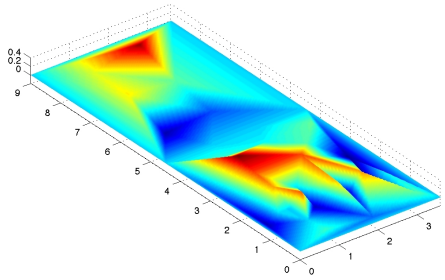

Figure 6.12: Mode shape at 45.8 Hz from measurements.

Figure 6.13 and 6.14 shows the deflection at 86.9 Hz in the model and at the highest obtained eigenfrequency (∼95 Hz) from measurements. These did not match at all in the vector analysis, but there is a very clear resemblance between the mode shape plots. Even if the complete deflection probably is not caught by the 31 accelerometers, the real structure and the model seem to behave in similar fashion in these two eigenmodes.

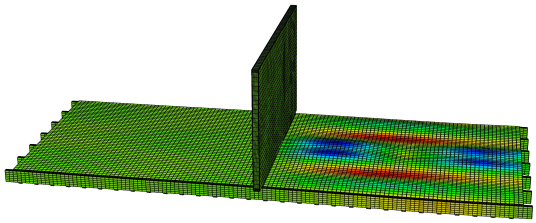

Figure 6.13: Mode shape at 86,9 Hz from simulations.

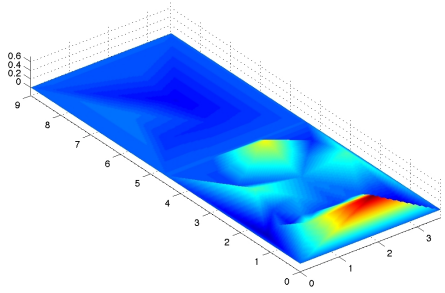

Figure 6.14: Mode shape at 92.3 Hz from measurements.

7. Concluding Remarks

The objective of creating a model that has the same dynamic behavior as the structure in terms of eigenfrequencies and mode shapes for frequencies up to 100 Hz turned out to be a bit optimistic since the displacement of the structure was too complicated to be measured with only 31 accelerometers for some of the higher frequencies. It is hard to analyse whether or not these eigenmodes were successfully reproduced in the FE-model. The aim was to simulate the lower eigenmodes and the first two eigenmodes showed great similarity in both frequency and mode shape between measurement and simulation. There were also a couple of eigenmodes from simulations at higher frequencies that were close to the measured eigenmodes in terms of frequencies and with obvious similarity in mode shapes.

When modeling a structure of such complexity as the floor-wall structure, there are many possible sources of error. But since a lot of effort was made to obtain a good model of a single beam (with satisfying result), the material properties of the floor beams and the boundary conditions between floor beams and supports is considered to be relatively accurate. However, errors may exist since the material properties can vary between the beams and the Young's modulus was only determined from experiments on one beam. The material properties of the other wood parts were not as well established as for the floor beams, but since they were not exposed to the same magnitude of forces and displacements the error is regarded as minor.

A major source of error when modeling an assembled structure may be how the connections between the different parts are modeled. For the floor-wall structure good results were obtained by simply letting all degrees of freedom on connecting surfaces be tied to each other. This was probably successful since the connections in the real structure were made very firm, for example the particle boards were both glued and screwed to the floor beams. If that would not have been the case, there would probably have been a need to experiment more with creating different partitionings of the surfaces or make special joint interfaces.

Unsymmetry of the real structure due to irregularities in the materials and the assemblage is another source of error. Before performing any experiments, the height of some supports had to be adjusted to make contact with the beams. Nevertheless, the forces on the supports will vary significantly.

When information was extracted about peak frequencies from the frequency sweep

measurements, the resolution of the RMS-plots was poor for the lower frequencies (more than 1 Hz for the lowest frequencies). In the simulations, the resolution was set to 0.25 Hz. This meant that there was no point in analysing the difference in frequencies down to decimals.

8. Proposal for Future Work

There are a lot of possible continuations to this project. First of all, there has been no time to examine the dynamic behaviour of the wall. Measurements with accelerometers on the wall were performed but not included in the report since there was no time to analyse them. Much more knowledge of the dynamic behaviour of the real structure could be obtained by performing more detailed measurements.

It would be interesting to excite the structure with loads from real life, such as footfalls or dropping objects, and examining the propagation of vibrations. The structure could also be used for acoustic research, for example how airborne sound propagate trough the structure.

In the model, further work could be done with developing more realistic interactions between the parts. If the dynamic behaviour of the wall were measured, the modeling of the floor-wall intersection would probably have to be improved to obtain resemblance.

A. Measurement Coordinates

Accelerometer nr.	**x-coordinate (m)**	**y-coordinate (m)**
0	0.0	2.25
2	0.6	2.25
3	1.2	2.25
4	1.8	2.25
5	2.4	2.25
6	3.0	2.25
7	3.6	2.25
8	0.0	4.50
9	0.6	4.50
10	1.2	4.50
11	1.8	4.50
12	2.4	4.50
13	3.0	4.50
14	3.6	4.50
15	0.9	7.03
16	2.7	7.03
17	0.9	1.00
18	2.7	1.00
19	0.9	3.11
20	2.7	3.11
40	0.0	6.75
41	0.6	6.75
42	1.2	6.75
43	1.8	6.75
44	2.4	6.75
45	3.0	6.75
46	3.6	6.75

Table A.1: Coordinates of the accelerometers used in measurements of the floor without particle boards.

Accelerometer nr.	**x-coordinate (m)**	**y-coordinate (m)**
0	0.9	0.3
2	2.1	0.3
3	3.3	0.3
4	0.6	0.9
5	0.3	1.5
40	0.6	1.5
7	0.9	1.5
41	1.2	1.5
9	1.5	1.5
42	1.8	1.5
11	2.1	1.5
43	2.4	1.5
13	2.7	1.5
44	3.0	1.5
15	3.6	1.5
6	0.9	2.1
8	1.5	2.1
10	0.9	2.7
12	2.1	2.7
26	3.3	2.7
14	0.9	3.3
16	2.7	3.3
17	0.9	3.9
18	2.1	3.9
19	3.3	3.9
20	0.9	5.7
21	2.1	5.7
22	0.9	6.9
23	2.1	6.9
24	0.9	8.1
25	2.1	8.1

Table A.2: Coordinates of the accelerometers used in the measurements of the floor.

Excitation	**x-coordinate (m)**	**y-coordinate (m)**
Transient 1	0.0	1.0
Transient 2	0.6	1.5
Transient 3	1.2	1.0
Transient 4	1.8	1.5

Table A.3: Coordinates of the excitation points used for the floor without particle boards.

Excitation	**x-coordinate (m)**	**y-coordinate (m)**
Frequency sweep 1	0.9	1.5
Frequency sweep 2	1.8	2.1
Frequency sweep 3	2.7	2.7
Transient 1	0.9	0.9
Transient 2	1.8	1.2
Transient 3	2.7	2.1

Table A.4: Coordinates of the excitation points used for the floor.

References

[1] Anil K. Chopra (1995). *Dynamics of structures.* Prentice Hall.

[2] Austrell, Per-Erik (2010). *Lecture notes: Dynamics of structures.* Division of Structural Mechanics.

[3] Ottosen N. S. & Petersson H. (1992). *Introduction to the finite element method.* Prentice Hall.

[4] Isaksson T. & Mårtensson A. (2008) *Byggkonstruktion, Regel- och formelsamling.* Studentlitteratur.

[5] SIMULIA (2008). *Abaqus manual 6.9.*

[6] Forskning & Framsteg: Flervåningshus av trä. *http://fof.se/textruta/flervaningshus-av-tra.* December 10^{th} 2010.

[7] SvD - Trähus minskar koldioxidutsläpp. *http://www.svd.se/nyheter/inrikes/trahus-minskar-koldioxidutslapp_857029.svd.* December 10^{th} 2010.

[8] Setra - Trälyftet. *http://www.setragroup.com/upload/Dokument/Produktbroschyrer/Tr%c3%a4lyftfolderSv.pdf.* December 10^{th} 2010.

[9] Akustik och vibrationer i lätta konstruktioner (4/2008). *http://www.sp.se/sv/areas/wood/buildinghousing/news/Sidor/default.aspx.* December 10^{th} 2010.

[10] Träguiden. *http://www.traguiden.se.* December 10^{th} 2010.

[11] Simulia - products. *http://www.simulia.com/products/products.html.* December 18^{th} 2010.

[12] Gyproc - Materialegenskaper. *http://www.gyproc.se/files/PDF/Sweden/mtrl_skiv_prodegen.pdf.* December 18^{th} 2010.

[13] Ph.D. Kent Person, Division of Structural Dynamics, Lund University.